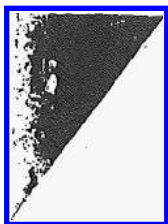


# **AIAA-81-1259** **Numerical Solutions of** **the Euler Equations by** **Finite Volume Methods Using** **Runge-Kutta Time-Stepping** **Schemes**

A. Jameson, Princeton University,  
Princeton, NJ; and  
W. Schmidt, Dornier GmbH,  
Friedrichshafen, FRG; and  
E. Turkel, University of Tel Aviv,  
Israel

**AIAA 14th Fluid and Plasma**  
**Dynamics Conference**

June 23-25, 1981/Palo Alto, California



# NUMERICAL SOLUTION OF THE EULER EQUATIONS BY FINITE VOLUME METHODS USING RUNGE KUTTA TIME STEPPING SCHEMES

A. Jameson\*

Department of Mechanical and Aerospace Engineering  
Princeton University  
Princeton, N.J. 08544

Wolfgang Schmidt<sup>t</sup>  
Dornier GmbH  
Friedrichshafen, W. Germany

Eli Turkel<sup>\*\*</sup>  
University of Tel Aviv  
Tel Aviv, Israel

## Abstract

A new combination of a finite volume discretization in conjunction with carefully designed dissipative terms of third order, and a Runge Kutta time stepping scheme, is shown to yield an effective method for solving the Euler equations in arbitrary geometric domains. The method has been used to determine the steady transonic flow past an airfoil using an O mesh. Convergence to a steady state is accelerated by the use of a variable time step determined by the local Courant number, and the introduction of a forcing term proportional to the difference between the local total enthalpy and its free stream value.

## 1. Introduction

While potential flow solutions have proved extremely useful for predicting transonic flows with shock waves of moderate strength<sup>(1)</sup>, typical of cruising flight of long range transport aircraft, the approximation of ignoring entropy changes and vorticity production cannot be expected to give acceptable accuracy when the flight speed is increased into the upper transonic range. There also appears to be some disturbing discrepancies between conservative potential flow solutions and solutions of the Euler equations at quite moderate Mach numbers, such as the NACA 0012 airfoil at Mach .8 and an angle of attack of 1.25°<sup>(2)</sup> (possibly related to the existence of non-unique solutions of the transonic potential flow equation<sup>(3)</sup>).

The purpose of the present work is to develop economical methods of solving the Euler equations, particularly for steady flows, with the aim of reducing the computational cost to the point where they might be used as an alternative to potential flow calculations for design work. Since it is desired that the methods should be applicable to complex geometric configurations, the finite volume formulation has been used to develop the space discretization, allowing the use of an arbitrary grid. This has the additional advantage that calculations can be performed on the same grids as have been used for potential flow calculations, so that errors due to the potential flow assumption can be assessed.

The research stems from a visit by the first author to the Dornier company in August 1980. At that time he substituted an alternative difference scheme into a code for solving the Euler equations which had been previously developed by Rizzi and Schmidt<sup>(4)</sup>. The new method retained the finite volume formulation of the earlier method, but replaced the MacCormack scheme by a three state iterated central difference scheme for advancing the solution at each time step, comparable to the schemes of Gary<sup>(5)</sup> and Stetter<sup>(6)</sup>. A key feature was the introduction of dissipative terms in a separate filter stage at the end of each time step. The magnitude of the dissipative terms was adapted to the local properties of the flow by means of a sensor based on the local pressure gradient.

The revised method was found to offer significant advantages over the MacCormack scheme. In particular the results of a linear stability analysis indicates that the scheme is stable for Courant numbers up to 2 in one dimensional problems, and that stability is maintained in multidimensional problems with an appropriately reduced time step, without any need for splitting. These properties have been confirmed in practice, and the scheme has been found in fact to be stable enough to allow a variable time step at the limit set by the local Courant number to be used throughout computational domains with very large variations in cell size. This permits steady states to be reached in a few hundred time steps even on O meshes, where the largest cells are many million times the size of the smallest cells clustered at the trailing edge. The scheme also has the advantage that by using central differences it treats the flow on the upper and lower sides of the airfoil symmetrically on O and C meshes, whereas the MacCormack scheme requires logic to preserve the same sequence of upwind and downwind differencing on the two sides of the airfoil.

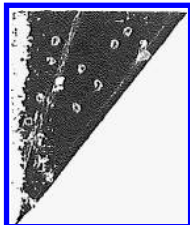
The implementation of the three stage central difference scheme for three dimensional flows has been carried out by Rizzi and is described in a separate paper<sup>(7)</sup>. In a concurrent effort the present authors have continued an investigation of alternative two dimensional schemes with the objective of finding answers to some of the following questions:

- (1) What is the most efficient time stepping scheme?
- (2) What is the optimal form of the dissipative terms?

\* Professor

\*\* Professor

<sup>t</sup> Chief of Theoretical Aerodynamics



- (3) What is the best way to treat the boundary conditions at the body and in the far field?
- (4) How can convergence to a steady state be accelerated?

It is concluded

- (1) that a fourth order Runge Kutta time stepping scheme is preferable to the three stage scheme.
- (2) that the dissipative terms should be constructed from an adaptive blend of second and fourth differences.
- (3) that the treatment of the boundary conditions in the far field should be based on the appropriate characteristic combinations of variables.
- (4) that convergence to a steady state is significantly accelerated
  - (a) by using a variable time step at the maximum limit set by the local Courant number
  - (b) by adding a forcing term based on the difference between the local total enthalpy and its free stream value (this implies that the energy equation must be integrated in time, and not eliminated in favor of the steady state condition that the total enthalpy is constant, as has been the practice in a number of recent applications (4,7,8)).

Some numerical results supporting these conclusions are presented in the last section. Applications of the method to practical aerodynamic problems are discussed in a companion paper, which addresses questions such as the inclusion of boundary layer corrections, treatment of the Kutta condition, and differences between potential flow and Euler solutions<sup>(9)</sup>.

## 2. Finite Volume Scheme

Let  $p$ ,  $\rho$ ,  $u$ ,  $v$ ,  $E$  and  $H$  denote the pressure, density, Cartesian velocity components, total energy and total enthalpy. For a perfect gas

$$E = \frac{p}{(\gamma-1)\rho} + \frac{1}{2}(u^2 + v^2), \quad H = E + \frac{p}{\rho} \quad (1)$$

where  $\gamma$  is the ratio of specific heats. The Euler equations for two dimensional inviscid flow can be written in integral form for a region  $\Omega$  with boundary  $\partial\Omega$  as

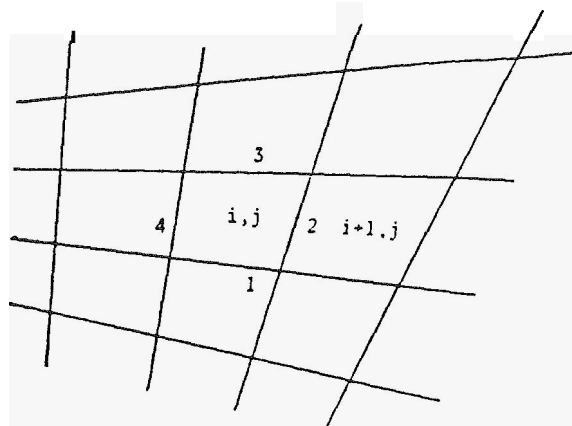
$$\frac{d}{dt} \iint_{\Omega} w \, dx \, dy + \oint_{\partial\Omega} (f \, dy - g \, dx) = 0 \quad (2)$$

where  $x$  and  $y$  are Cartesian coordinates and

$$w = \begin{pmatrix} \rho \\ \rho u \\ \rho v \\ \rho E \end{pmatrix}, \quad f = \begin{pmatrix} \rho u \\ \rho u^2 + p \\ \rho uv \\ \rho uH \end{pmatrix}, \quad g = \begin{pmatrix} \rho v \\ \rho vu \\ \rho v^2 + p \\ \rho vH \end{pmatrix} \quad (3)$$

The discretization procedure follows the method of lines in decoupling the approximation of the spatial and Temporal terms. The computational domain is divided into quadrilateral cells as in the sketch, and a system of ordinary differential equations is obtained by applying equation (2) to each cell separately. The resulting equations can then be

solved by several alternative time stepping schemes.



Let the values of the quantities associated with each cell be denoted by  $i,j$ . (These can be regarded as values at the cell center, or average values for the cell). For each cell equation (2) assumes the form

$$\frac{d}{dt} (hw) + Qw = 0 \quad (4)$$

where  $h$  is the cell area, and the operator  $Q$  represents an approximation to the boundary integral defined by the second term of (2). This is defined as follows. Let  $\Delta x_k$  and  $\Delta y_k$  be the increments of  $x$  and  $y$  along side  $k$  of the cell, with appropriate signs. Then the flux balance for, say, the  $x$  momentum component, is represented as

$$\frac{d}{dt} (h\rho) + \sum_{k=1}^4 (Q_k \rho u_k + \Delta y_k p_k) = 0 \quad (5)$$

where  $h$  is the cell area,  $Q_k$  is the flux velocity

$$Q_k = \Delta y_k u_k - \Delta x_k v_k \quad (6)$$

and the sum is over the four sides of the cell. Each quantity such as  $u_k$  or  $(\rho u)_k$  is evaluated as the average of the values in the cells on the two sides of the face,

$$(\rho u)_k = \frac{1}{2} (\rho u)_{i,j} + \frac{1}{2} (\rho u)_{i+1,j} \quad (7)$$

For example. The scheme reduces to a central difference scheme on a Cartesian grid, and is second order accurate provided that the grid is smooth enough.

## 3. Dissipative Terms

To suppress the tendency for odd and even point decoupling, and to prevent the appearance of wiggles in regions containing severe pressure gradients in the neighborhood of shock waves or stag-



nation points, it proves necessary to augment the finite volume scheme by the addition of artificial dissipative terms. Therefore equation (4) is replaced by the equation

$$\frac{d}{dt} (hw) + Qw - Dw = 0 \quad (8)$$

where  $Q$  is the spatial discretization operator defined by equations (5-7), and  $D$  is a dissipative operator. Extensive numerical experiments have established that an effective form for  $Dw$  is a blend of second and fourth differences with coefficients which depend on the local pressure gradient.

The construction of the dissipative terms for each of the four dependent variables is similar. For the density equation

$$Dp = D_X p + D_Y p \quad (9)$$

where  $D_X p$  and  $D_Y p$  are corresponding contributions for the two coordinate directions, written in conservation form

$$\begin{aligned} D_X p &= d_{i+\frac{1}{2},j} - d_{i-\frac{1}{2},j} \\ D_Y p &= d_{i,j+\frac{1}{2}} - d_{i,j-\frac{1}{2}} \end{aligned} \quad (10)$$

The terms on the right all have a similar form; for example

$$d_{i+\frac{1}{2},j} = h_{i+\frac{1}{2},j} \left\{ \begin{aligned} &\epsilon_{i+\frac{1}{2},j}^{(2)} (p_{i+1,j} - p_{i,j}) \\ &-\epsilon_{i+\frac{1}{2},j}^{(4)} (p_{i+2,j} - 3p_{i+1,j} \\ &\quad + 3p_{i,j} - p_{i-1,j}) \end{aligned} \right\} \quad (11)$$

where  $h$  is the cell volume, and the coefficients  $\epsilon^{(2)}$  and  $\epsilon^{(4)}$  are adapted to the flow. Define

$$v_{i,j} = \frac{|p_{i+1,j} - 2p_{i,j} + p_{i-1,j}|}{|p_{i+1,j}| + 2|p_{i,j}| + |p_{i-1,j}|} \quad (12)$$

Then

$$\epsilon_{i+\frac{1}{2},j}^{(2)} = \kappa^{(2)} \max(v_{i+1,j}, v_{i,j}) \quad (13)$$

and

$$\epsilon_{i+\frac{1}{2},j}^{(4)} = \max\left(0, (\kappa^{(4)} - \epsilon_{i+\frac{1}{2},j}^{(2)})\right) \quad (14)$$

where typical values of the constants  $\kappa^{(2)}$  and  $\kappa^{(4)}$  are

$$\kappa^{(2)} = \frac{1}{4}, \quad \kappa^{(4)} = \frac{1}{256}$$

The dissipative terms for the remaining equations are obtained by substituting  $\rho u$ ,  $\rho v$  and either  $\rho E$  or  $\rho H$  for  $p$  in these formulas.

The scaling  $h/\Delta t$  in equation (11) conforms to the inclusion of the cell area  $h$  in the dependent variables of equation (8). Since equation (11) contains undivided differences, it follows that if  $\epsilon^{(2)} = O(\Delta x^2)$  and  $\epsilon^{(4)} = O(1)$ , then the added terms are of order  $\Delta x^3$ . This will be the case in a region where the flow is smooth. Near a shock wave  $\epsilon^{(2)} = O(1)$ , and the scheme behaves locally like a first order accurate scheme.

It has been found that in smooth regions of the flow, the scheme is not sufficiently dissipative unless the fourth differences are included, with the result that calculations will generally not converge to a completely steady state. Instead, after they have reached an almost steady state, oscillations of **very** low amplitude continue indefinitely (with  $\max \frac{\partial \rho}{\partial t} \sim 10^3$ , for example).

These appear to be induced by reflections from the boundaries of the computational domain. Near shock waves it has been found that the fourth differences tend to induce overshoots, and therefore they are switched off by subtracting  $\epsilon^{(2)}$  from  $\kappa^{(4)}$  in equation (14).

#### 4. Time Stepping Schemes

Stable time stepping methods for equation (8) can be patterned on standard schemes for ordinary differential equations. Multistage two level schemes of the Runge Kutta type have the advantage that they do not require any special starting procedure, in contrast to leap frog and Adams Bashforth methods, for example. The extra stages can be used either

- (1) to improve accuracy, or
- (2) to extend the stability region.

An advantage of this approach is that the properties of these schemes have been widely investigated, and are readily available in textbooks on ordinary differential equations.

Consider a linear system of equations

$$\frac{dw}{dt} + Aw = 0.$$

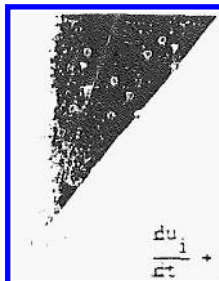
Suppose that  $A$  can be expressed as  $A = T\Lambda T^{-1}$  where  $T$  is the matrix of the eigenvectors of  $A$ , and  $\Lambda$  is diagonal. Then setting  $v = T^{-1}w$  yields separate equations

$$\frac{dv_k}{dt} + \lambda_k v_k = 0$$

for each dependent variable  $v_k$ . The stability region is that region of the complex plane containing values of  $\lambda \Delta t$  for which the scheme is stable. Consider now the model problem

$$\frac{\partial u}{\partial t} + a \frac{\partial u}{\partial x} + \epsilon \Delta x \frac{\partial^2 u}{\partial x^2} = 0 \quad (15)$$

on a uniform mesh with interval  $\Delta x$ , with a dissipative term of order  $\Delta x$ . This can be reduced to a system of ordinary differential equations by introducing central-difference approximations for  $\frac{\partial}{\partial x}$  and  $\frac{\partial^2}{\partial x^2}$ :



$$\frac{du}{dt} + \frac{a}{\Delta x} (u_{i+1} - u_{i-1}) + \frac{\epsilon}{\Delta x} (u_{i+1} - 2u_i - u_{i-1}) = 0$$

Taking the Fourier transform in space

$$\hat{u} = \frac{1}{2\pi} \int_{-\infty}^{\infty} u e^{i\omega x} dx$$

this becomes

$$\frac{d\hat{u}}{dt} + \lambda \hat{u} = 0$$

where

$$\lambda = \frac{1}{\Delta x} (i a \sin \omega \Delta x - 4\epsilon \sin^2 \frac{\omega \Delta x}{2})$$

It can be seen that the maximum allowable value of the imaginary part of  $\lambda \Delta t$  determines the maximum value of the Courant number  $a \Delta t / \Delta x$  for which the calculation will be stable, while the addition of the dissipative term shifts the region of interest to the left of the imaginary axis.

In the present case, if the grid is held fixed in time so that the cell area  $h$  is constant, the system of equations (8) has the form

$$\frac{dw}{dt} + Pw = 0 \quad (16)$$

where if  $Q$  is the discretization operator defined in Section 2, and  $D$  is the dissipative operator defined in Section 3, the nonlinear operator  $P$  is defined as

$$Pw \equiv \frac{1}{h} (Qw - Dw) \quad (17)$$

The investigation has concentrated on two time stepping schemes. The first is a three stage scheme which is defined as follows. Let a superscript  $n$  denote the time level, and let  $\Delta t$  be the time step. Then at time level  $n$  set

$$\begin{aligned} w^{(0)} &= w^n \\ w^{(1)} &= w^{(0)} - \Delta t Pw^{(0)} \\ w^{(2)} &= w^{(0)} - \frac{\Delta t}{2} (Pw^{(0)} + Pw^{(1)}) \\ w^{(3)} &= w^{(0)} - \frac{\Delta t}{2} (Pw^{(0)} + Pw^{(2)}) \\ w^{n+1} &= w^{(3)} \end{aligned} \quad (18)$$

Variations of this scheme have been proposed by Gary<sup>(5)</sup>, Stetter<sup>(6)</sup>, and Graves and Johnson<sup>(10)</sup>. It can be regarded as a Crank Nicolson scheme with a fixed point iteration to determine the solution at time level  $n+1$ , and the iterations terminated after the third iteration. It is second order accurate in time, and for the model problem (15) with  $\epsilon=0$ , it is stable when the Courant number

$$\left| \frac{a \Delta t}{\Delta x} \right| < 2$$

This bound is not increased by additional iterations. Compared with standard third order Runge Kutta

schemes, this scheme gives up third order accuracy in time for a larger bound on the Courant number.

The other scheme which has been extensively investigated is the classical fourth order Runge Kutta scheme, defined as follows. At time level  $n$  set

$$\begin{aligned} w^{(0)} &= w^n \\ w^{(1)} &= w^{(0)} - \frac{\Delta t}{2} Pw^{(0)} \\ w^{(2)} &= w^{(0)} - \frac{\Delta t}{2} Pw^{(1)} \\ w^{(3)} &= w^{(0)} - \Delta t Pw^{(2)} \\ w^{(4)} &= w^{(0)} - \frac{\Delta t}{6} (Pw^{(0)} + 2Pw^{(1)} + 2Pw^{(2)} + Pw^{(3)}) \\ w^{n+1} &= w^{(4)} \end{aligned} \quad (19)$$

This scheme is fourth order accurate in time, and for the model problem (15) with  $\epsilon=0$ , it is stable for Courant numbers

$$\left| \frac{a \Delta t}{\Delta x} \right| < 2\sqrt{2}$$

Its stability region, which is displayed on page 176 of Ref. (11), for example, also extends well to the left of the imaginary axis, allowing latitude in the introduction of dissipative terms.

Both schemes have the property that if  $Pw^n = 0$  then  $w^{(1)} = w^{(0)}$ , and so on, so that  $w^{n+1} = w^n$ , and the steady state solution is

$$Pw = 0$$

independent of the time step  $\Delta t$ . This allows a variable time step determined by the bound on the local Courant number to be used to accelerate convergence to a steady state without altering the steady state.

The expense of re-evaluating the dissipative terms at every stage of these schemes is substantial. One method of avoiding this is to introduce the dissipative terms in a separate fractional step after the last stage of the Runge Kutta scheme. Then equation (17) is replaced by

$$Pw \equiv \frac{1}{h} Qw \quad (17')$$

and the fourth order Runge Kutta scheme defined by equation (19), for example, is modified by setting

$$w^{n+1} = w^{(4)} + \Delta t D w^{(4)}$$

This method has the advantage that the stability properties for the two fractional steps are independent, so that the scheme will be stable if each fractional step is stable. It has the disadvantage that the steady state solution is no longer independent of the time step.

An alternative approach which has proved successful in practice, is to freeze the dissipative terms at their values in the first stage. Thus the fourth order Runge Kutta scheme is modified so that it has the form

$$\begin{aligned}
 w^{(0)} &= w^n \\
 w^{(1)} &= w^{(0)} - \frac{\Delta t}{2h} Q_w^{(0)} + \frac{\Delta t}{2h} D_w^{(0)} \\
 w^{(2)} &= w^{(0)} - \frac{\Delta t}{2h} Q_w^{(1)} + \frac{\Delta t}{2h} D_w^{(0)} \\
 w^{(3)} &= w^{(0)} - \frac{\Delta t}{h} Q_w^{(2)} + \frac{\Delta t}{h} D_w^{(0)} \\
 w^{(4)} &= w^{(0)} - \frac{\Delta t}{6h} (Q_w^{(0)} + 2Q_w^{(1)} + 2Q_w^{(2)} + Q_w^{(3)}) \\
 &\quad + \frac{\Delta t}{h} D_w
 \end{aligned} \quad (20)$$

The operators  $Q$  and  $D$  require roughly equal amounts of computation. Assigning to each 1 unit of work, and assuming that dissipative terms would be required in the leap frog or MacCormack schemes, both of which have maximum time steps bounded by a Courant number of one, one obtains the following table for the relative efficiency of the schemes:

Scheme	Evaluations of $Q$	Evaluations of $D$	Work	Maximum Courant Number	Efficiency = time step / work
Leap frog	1	1	2	1	1/2
MacCormack	2	1	3	1	1/3
3 stage	3	3	6	2	1/3
4 stage	4	4	8	2.8	.35
4 stage	4	1	5	2.8	.56

(frozen  $D$ )

## 5. Boundary Conditions

Improper treatment of the boundary conditions can lead to serious errors and perhaps instability. In order to treat the flow exterior to a profile one must introduce an artificial outer boundary to produce a bounded domain. If the flow is subsonic at infinity there will be three incoming characteristics where there is inflow across the boundary, and one outgoing characteristic, corresponding to the possibility of escaping acoustic waves. Where there is outflow, on the other hand, there will be three outgoing characteristics and one incoming characteristic. According to the theory of Kreiss<sup>(12)</sup>, three conditions may therefore be specified at inflow, and one at outflow, while the remaining conditions are determined by the solution of the differential equation. It is not correct to specify free stream conditions at the outer boundary.

For the formulation of the boundary conditions it is convenient to assume a local transformation to coordinates  $X$  and  $Y$  such that the boundary coincides with a line  $Y = \text{constant}$ . Using subscripts  $X$  and  $Y$  to denote derivatives, the Jacobian

$$h = x_X y_Y - x_Y y_X \quad (21)$$

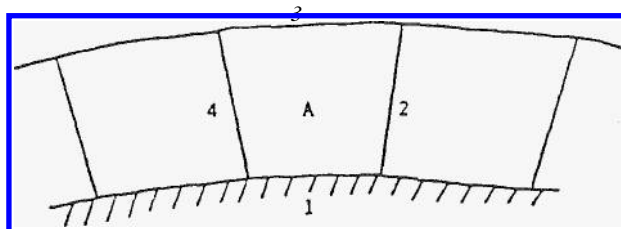
corresponds to the cell area of the finite volume scheme. Introduce the transformed flux vectors

$$F = y_Y f - x_Y g, \quad G = x_X g - y_X f \quad (22)$$

where  $f$  and  $g$  are defined by equation (3). In differential form equation (2) then becomes

ferential form equation (2) then becomes

$$\frac{\partial}{\partial t} (hw) + \frac{\partial F}{\partial X} + \frac{\partial G}{\partial Y} = 0 \quad (23)$$



Consider first the boundary condition at the profile. Across side 1 of cell  $A$  in the sketch there is no convected flux since

$$x_X v - y_X u = 0 \quad (24)$$

But there are contributions  $\Delta p$  and  $\Delta p$  to the momentum equations, which require an estimate of the pressure at the wall. Taking the time derivative of equation (24) multiplied by  $\rho$ , and substituting for  $\frac{\partial}{\partial t} (hpu)$  and  $\frac{\partial}{\partial t} (hpv)$  from equation (23) leads to the relation (given by Rizzi<sup>(13)</sup>)

$$(x_X^2 + y_X^2) p_Y = (x_X x_Y + y_X y_Y) p_X + \rho (y_Y u - x_Y v) (v x_{XX} + u y_{XX}) \quad (25)$$

Thus we can estimate  $p_Y$  in terms of quantities which can be determined from the interior solution, and we can use this value of  $p_Y$  to extrapolate the pressure from the adjacent cell center to the wall.

Stable boundary conditions have been given by Gottlieb and Turkel<sup>(14)</sup> and Gustafsson and Olinger<sup>(15)</sup> for a variety of difference schemes. The treatment of the outer boundary condition adopted here follows similar lines. The equations are linearized about values at the end of the previous time step, and the characteristic variables corresponding to outgoing characteristics are then determined by extrapolation from the interior, while the remaining boundary conditions are specified in a manner consistent with the conditions imposed by the free stream. Let

$$A = \frac{\partial F}{\partial w}, \quad B = \frac{\partial G}{\partial w}$$

Since the boundary is a line  $Y = \text{constant}$ , the eigenvalues of  $B$  determine the incoming and outgoing Characteristics. If  $q$  and  $q_t$  are the velocity components normal and tangential to the boundary, and  $c$  is the speed of sound, these eigenvalues are  $q_n$ ,  $q_t$ ,  $q_n - c$ , and  $q_n + c$ . Let values at the end of the previous time step be denoted by the subscript 0, and let  $T_0$  be the eigenvector matrix of  $B_0$ . Then  $B_0$  is reduced to diagonal form by the transformation  $A_0 = T_0^{-1} B_0 T_0$ , and setting  $v = T_0^{-1} w$ , the linearized equation assumes the form

$$\frac{\partial}{\partial t} (hv) + T_0^{-1} A_0 T_0 \frac{\partial v}{\partial X} + A_0 \frac{\partial v}{\partial Y} = 0$$

The characteristic variables are the components of  $v$ . These are  $p - c_o^2 \rho$ ,  $q_t$ ,  $p - \rho_o c_o q_n$  and  $p_o + \rho_o c_o q_n$ .

Let values extrapolated from the interior and free stream values be denoted by the subscripts  $e$  and  $\infty$ . Then at the inflow boundary we set

$$p - c_o^2 \rho = p_\infty - c_o^2 \rho_\infty \quad (26a)$$

$$q_t = q_{t_\infty} \quad (26b)$$

$$p - \rho_o c_o q_n = p_\infty - \rho_o c_o q_{n_\infty} \quad (26c)$$

$$p + \rho_o c_o q_n = p_e + \rho_o c_o q_{n_e} \quad (26d)$$

yielding

$$p = \frac{1}{2} (p_e + p_\infty - \rho_o c_o (q_{n_e} - q_{n_\infty}))$$

$$q_n = q_{n_\infty} + \frac{p - p_\infty}{\rho_o c_o}$$

The density can be determined from (26a). For steady state calculations it can alternatively be determined by specifying that the total enthalpy  $H$  has its free stream value.

At the outflow boundary one condition should be specified. If the flow is a parallel stream then  $\frac{\partial p}{\partial y} = 0$ , so for an open domain

$$p = p_\infty \quad (27)$$

A non reflecting boundary condition which would eliminate incoming waves is

$$\frac{\partial}{\partial t} (p - \rho_o c_o q_n) = 0 \quad (28)$$

This does not assure (27). Following Rudy and Strikwerda<sup>(16)</sup>, (27) and (28) are therefore combined as

$$\frac{\partial}{\partial t} (p - \rho_o c_o q_n) + \alpha (p - p_\infty) = 0 \quad (29)$$

where a typical value of the parameter  $\alpha$  is  $1/8$ . The velocity components and energy are extrapolated from the interior.

Various other boundary conditions designed to reduce reflections from the outer boundary have been proposed by several authors<sup>(17,18)</sup>, and it seems that it would be worth while to test some of these alternatives.

## 6. Convergence Acceleration

Two devices have been used to accelerate the convergence of the solutions to a steady state. The first is to use the largest possible time step permitted by the local stability bound everywhere in the computational domain. This has the effect of assuring that disturbances are propagated the whole way across the domain in a number of time steps of the same order as the number of mesh in-

tervals. It can be regarded as scaling the wave speed to give equations of the form

$$\frac{\partial w}{\partial t} + \lambda \left( \frac{\partial f}{\partial x} + \frac{\partial g}{\partial y} \right) = 0$$

where  $\lambda$  is proportional to the local mesh interval. Assuming that a stretched grid is used to extend the computational domain away from the profile,  $\lambda$  will be very large near the outer edge of the domain.

As a model for this procedure consider the wave equation in polar coordinates  $r$  and  $\theta$ ,

$$\phi_{tt} = c^2 \left( \frac{1}{r} \frac{\partial}{\partial r} (r \phi_r) + \frac{1}{r^2} \phi_{\theta\theta} \right)$$

Suppose that the wave speed  $c$  is proportional to the radius, say  $c = \alpha r$ . Then

$$\phi_{tt} = \alpha^2 \left( r \frac{\partial}{\partial r} (r \phi_r) + \phi_{\theta\theta} \right)$$

This has solutions of the form

$$\phi = \frac{1}{r^h} e^{-\alpha n t}$$

suggesting the possibility of exponential decay.

A more sophisticated modification of the equations, which is presently being investigated, is to set

$$\frac{\partial w}{\partial t} + M \left( \frac{\partial f}{\partial x} + \frac{\partial g}{\partial y} \right) = 0$$

where the matrix  $M$  couples the equations for  $\rho$ ,  $\rho u$ ,  $\rho v$  and  $\rho E$ , and modifies the eigenvalues of the system.

The second device for convergence acceleration is to introduce a forcing term proportional to the difference between the total enthalpy  $H$  and its free stream value  $H_\infty$ . In a steady flow with a uniform free stream  $H = H_\infty$  throughout the domain. The density and energy equations

$$\frac{\partial}{\partial x} (\rho u) + \frac{\partial}{\partial y} (\rho v) = 0$$

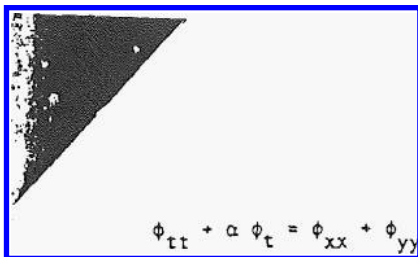
and

$$\frac{\partial}{\partial x} (\rho u H) + \frac{\partial}{\partial y} (\rho v H) = 0$$

are then consistent. This property is not preserved by various predictor corrector difference schemes, such as the MacCormack scheme. It is preserved by the schemes defined in sections 2-4, however, provided that the dissipative operator is applied to  $\rho H$  and not  $\rho E$  in the energy equation. Thus a forcing term proportional to  $H - H_\infty$  does not alter the steady state.

The reason for introducing such a term is to provide additional damping. The term is intended to have an effect similar to that of the term containing  $\phi_t$  in the telegraph equation:





$$\phi_{tt} + \alpha \phi_t = \phi_{xx} + \phi_{yy}$$

Multiplying this equation by  $\phi_t$ , and integrating by parts over all space leads to the relation

$$\frac{\partial P}{\partial t} + \alpha \int_{-\infty}^{\infty} \int_{-\infty}^{\infty} \phi_t^2 dx dy = 0$$

where

$$P = \frac{1}{2} \int_{-\infty}^{\infty} \int_{-\infty}^{\infty} (\phi_t^2 + \phi_x^2 + \phi_y^2) dx dy$$

Since  $P$  is non negative, it must decay if  $\alpha > 0$  until  $\phi = 0$ . When relaxation methods are regarded as simulating time dependent equations, it is similarly found that the term containing  $\phi_t$  plays a critical role in determining the rate of convergence (19).

In subsonic flow the Euler equations are equivalent to the unsteady potential flow equation

$$\phi_{tt} + 2u\phi_{xt} + 2v\phi_{yt} = (c^2 - u^2)\phi_{xx} - 2uv\phi_{xy} + (c^2 - v^2)\phi_{yy} \quad (30)$$

which can be reduced to the wave equation by introducing moving coordinates  $x' = x - ut$ ,  $y' = y - vt$ . Also the unsteady Bernoulli equation is

$$\phi_t + H = H_\infty$$

It can be verified that if the Euler equations are written in primitive form, and the density equation is modified by the addition of a term proportional to  $H - H_\infty$ , so that it becomes

$$\frac{\partial \rho}{\partial t} + u \frac{\partial \rho}{\partial x} + v \frac{\partial \rho}{\partial y} + \rho \left( \frac{\partial u}{\partial x} + \frac{\partial v}{\partial y} \right) + \alpha \rho (H - H_\infty) = 0$$

then the flow remains irrotational in the absence of shock waves, and equation (30) is modified by a term proportional to  $\phi_t$ . When the density equation is combined with the momentum equations to yield a system of equations in conservation form, the modified equations become

$$\begin{aligned} \frac{\partial \rho}{\partial t} + \frac{\partial}{\partial x}(\rho u) + \frac{\partial}{\partial y}(\rho v) + \alpha \rho (H - H_\infty) &= 0 \\ \frac{\partial}{\partial t}(\rho u) + \frac{\partial}{\partial x}(\rho u^2 + p) + \frac{\partial}{\partial y}(\rho uv) + \alpha \rho u (H - H_\infty) &= 0 \\ \frac{\partial}{\partial t}(\rho v) + \frac{\partial}{\partial x}(\rho uv) + \frac{\partial}{\partial y}(\rho v^2 + p) + \alpha \rho v (H - H_\infty) &= 0 \\ \frac{\partial}{\partial t}(\rho E) + \frac{\partial}{\partial x}(\rho u H) + \frac{\partial}{\partial y}(\rho v H) + \alpha \rho H (H - H_\infty) &= 0 \end{aligned}$$

The energy equation now has a quadratic term in  $H$ , like a Riccati equation. This can be destabilizing, and an alternative which has been found effective in practice is to modify the energy equation to the form

$$\frac{\partial}{\partial t}(\rho E) + \frac{\partial}{\partial x}(\rho u H) + \frac{\partial}{\partial y}(\rho v H) + \alpha (H - H_\infty) = 0$$

which tends to drive  $H$  towards  $H_\infty$ . The additional terms can conveniently be introduced in a separate fractional step at the end of each time step.

## 7. Results

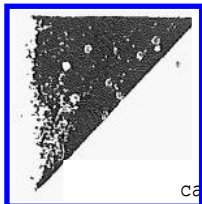
Some typical results of numerical calculations are presented in this section. Since the purpose is primarily to show the accuracy and convergence of the basic numerical algorithm, the examples are restricted to nonlifting flow past a cylinder and a NACA 0012 airfoil. Only the flow in the upper half plane was calculated, and an O mesh was used with 64 intervals in the chord wise direction and 32 intervals in the normal direction. The mesh extended to a distance of about 25 chords from the profile, and the mesh interval near the outer boundary was of the order of a chord. In the case of the NACA 0012 airfoil, the cells adjacent to the outer boundary had an area 2.5 million times greater than the area of the smallest cell, located at the trailing edge. Extensive numerical experiments confirmed the superior efficiency of the modified fourth order Runge Kutta scheme defined by equation (20), and this scheme was used to produce all the results displayed in this section.

Figure 1 shows results for flow past a circular cylinder. The grid is displayed in Figure 1(a). Figures 1(b) and 1(c) show the computed pressure distributions for Mach numbers of .35 and .45. The flow is fully subsonic in the first case, and there should be no departure from fore and aft symmetry in an exact calculation. The flow should also be isentropic. The calculations are normalized with  $p=1$  and  $\rho=1$  at infinity, so the quantity  $S=p/\rho^\gamma-1$  can be used as a measure of entropy generation. The largest computed value of  $S$  was .0003, at a point along the surface. At Mach .45 there is a moderately strong shock wave, as can be seen. The entropy was computed to be .0120 behind the shock wave. Figure 1(d) shows the convergence history for the flow at Mach .45. The measure of convergence is the residual for the density, defined as the root mean square value of  $\frac{\partial \rho}{\partial t}$  (calculated at

as  $\Delta \rho / \Delta t$  for the complete time step). This was reduced from 1.67 to .486  $10^{-3}$  in 1000 cycles. The mean rate of convergence was .978 per cycle. Another measure of convergence (not plotted) is the root mean square deviation of the total enthalpy from its free stream value. This was reduced from .0828 to .500  $10^{-3}$ . Enthalpy damping was used in this calculation to accelerate convergence. The calculation was started impulsively by suddenly introducing the cylindrical obstacle into a uniform flow, and immediately enforcing the solid wall boundary condition at its surface. This creates very large disturbances, but the pattern of the flow field is still quite rapidly established. One measure of this is the size of the supersonic zone. In this case the number of supersonic points was frozen after 450 cycles.

Figure 2 shows a comparison between the results of potential flow and Euler calculations for a NACA 0012 airfoil at zero degrees angle of attack and Mach .850. The mesh is shown in Figure 2(a), the potential flow result is shown in Figure 2(b), and the Euler result is shown in Figure 2(c). It





can be seen that the shock wave is further aft in the potential flow calculation, which was performed by the fully conservative finite volume method of Jameson and Caughey<sup>(20)</sup>, using a first order accurate formulation in the supersonic zone. The convergence history of the Euler calculation is shown in Figure 2(d). Figures 3(a) and 3(b) show a similar comparison between the potential flow and Euler results for the NACA 0012 airfoil at Mach .800. In this case the shock locations are identical. Figures 3(c) and 3(d) show the convergence history over 1500 cycles with and without enthalpy damping. Without enthalpy damping the final residual is  $.269 \cdot 10^{-6}$ . With enthalpy damping it is  $.240 \cdot 10^{-9}$ . These runs used the potential flow result as the starting condition for the Euler calculation. Thus the flow pattern was already essentially established at the start of the Euler calculation, with the result that the number of points in the supersonic zone was frozen after 180 cycles when enthalpy damping was used. To illustrate the development of the flow field without the assistance of the potential flow calculation, Figure 4 shows the result for the same flow after 200, 400, 600 and 800 cycles with an impulsive start. Finally a print out of the computed density, velocity components, total enthalpy, pressure, Mach number, and entropy (measured as  $S > p/pY-1$ ) is displayed in Figure 5. In an exact calculation S would be zero upstream of the shock wave. Actually it has a value of .0017 near the leading edge. Then it settles to values in the range of .0002 to .0009 ahead of the shock wave, and rises to .0054 behind the shock wave.

These results support the conclusions stated in the introduction. It also appears that shock waves can be satisfactorily captured without resorting to flux vector splitting and one sided differencing<sup>(21-24)</sup>, at least for steady state calculations, and that fairly rapid convergence to a steady state can be obtained without the use of an implicit scheme.

Attractive features of the scheme are its comparative simplicity, and its susceptibility to the extensive use of vector operations on a vector computer. The present implementation of the fourth order Runge Kutta scheme requires 426 floating point operations at each interior cell. On a mesh with  $64 \times 32 = 2048$  cells a single cycle therefore requires about .9 megaflops (million floating point operations). In tests on a Cray 1 computer it has been found that the program operates at 44 cycles per second (corresponding to a computing speed of about 40 megaflops per second). The code is written in standard FORTRAN, and this rate was achieved simply by relying on the capability of the Cray FORTRAN computer to vectorize the code automatically. A still higher rate could be realized by writing certain critical segments of the program in assembly language. In practice a typical run is more than sufficiently converged for engineering applications within 500 cycles. At 44 cycles a second such a calculation would be completed in 12 seconds, (or 24 seconds for a lifting case with twice as many mesh cells to represent the flow in both the upper or lower half planes, provided that the same rate of convergence could be realized).

#### 8. Acknowledgements

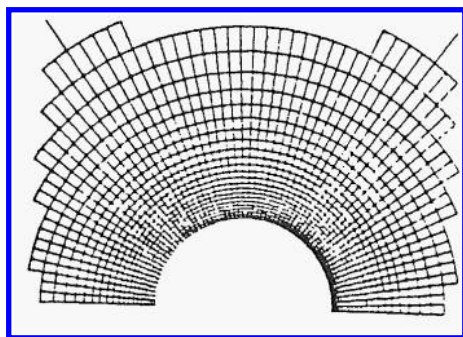
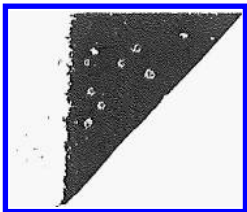
This work was supported by the Office of

Naval Research under Contract N00014-81-X-0379 and by NASA under Contract NAG2-96.

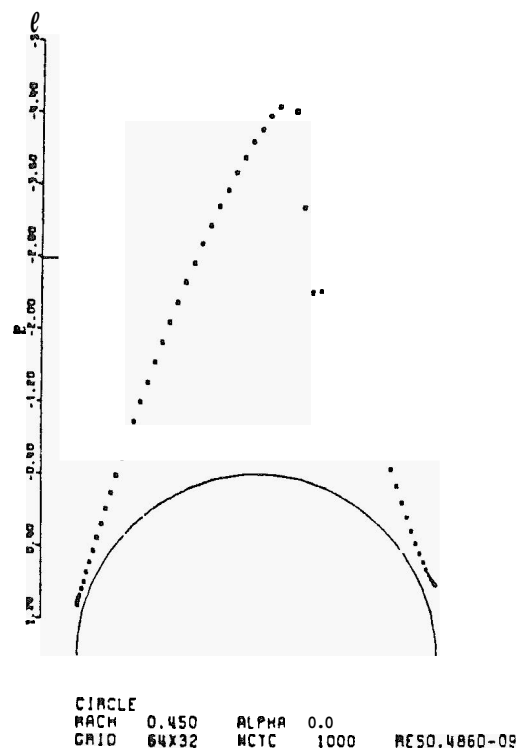
#### References

1. Jameson, A. "Numerical Calculation of Transonic Flow with Shock Waves". *Symposium Transsonicum II*, Gottingen, 1975, Springer-Verlag, 1976.
2. Rizzi, A., and Viviand, H. (editors), "Numerical Methods for the Computation of Inviscid Transonic Flow with Shocks", *Proceedings of GAMM Workshop*, Stockholm, 1979, Vieweg Verlag, 1981.
3. Steinhoff, J. and Jameson, A. "Multiple Solutions of the Transonic Potential Flow Equation", *Fifth AIAA Computational Fluid Dynamics Conference*, Palo Alto, 1981.
4. Rizzi, A. "Computation of Rotational Transonic Flow, in *Numerical Methods for the Computation of Inviscid Transonic Flow with Shocks*", *Proceedings of GAMM Workshop*, Stockholm, 1979, Vieweg Verlag, 1981.
5. Gary, J. "On Certain Finite Difference Schemes for Hyperbolic Systems", *Math. Comp.*, Vol. 18, pp. 1-18, 1964.
6. Stetter, H.J. "Improved Absolute Stability of Predictor-Corrector Schemes", *Computing*, Vol. 3, pp. 286-296, 1968.
7. Rizzi, A. and Eriksson, L.E. "Transfinite West Generation and Damped Euler Equation Algorithm for Transonic Flow Around Xing-body Configurations", *Fifth AIAA Computational Fluid Dynamics Conference*, Palo Alto, 1981.
8. Viviand, H. "Pseudo Unsteady Methods for Transonic Flow Computations", *Proceedings of Seventh International Conference on Numerical Methods in Fluid Dynamics*, Stanford, 1980, Springer-Verlag. 1981.
9. Jameson, A., Rizzi, A., Schmidt, W., and Whitfield, D. "Finite Volume Solution for the Euler Equation for Transonic Flow over Airfoils and Wings Including Viscous Effects", *AIAA Paper 81-1265*, 1981.
10. Graves, R. and Johnson, N. "Navier Stokes Solutions Using Stetter's Method", *AIM Journal*, Vol. 16, pp. 1013-1015, 1978.
11. Stetter, H.J. "Analysis of Discretization Methods for Ordinary Differential Equations", *Springer-Verlag*. 1973.
12. Kreiss, H.O. "Initial Boundary Value Problems for Hyperbolic Systems", *Comm. Pure Appl. Math.*, Vol. 23, pp. 217-290, 1970.
13. Rizzi, A. "Numerical Implementation of Solid Body Boundary Conditions for the Euler Equations", *ZAMM* Vol. 58, pp. 301-304, 1978.
14. Gocklieb, D. and Turkel, E. "Boundary Conditions for Multistep Finite Difference Methods for Time Dependent Equations", *J. Computational Physics*, Vol. 26, pp. 181-196, 1978.

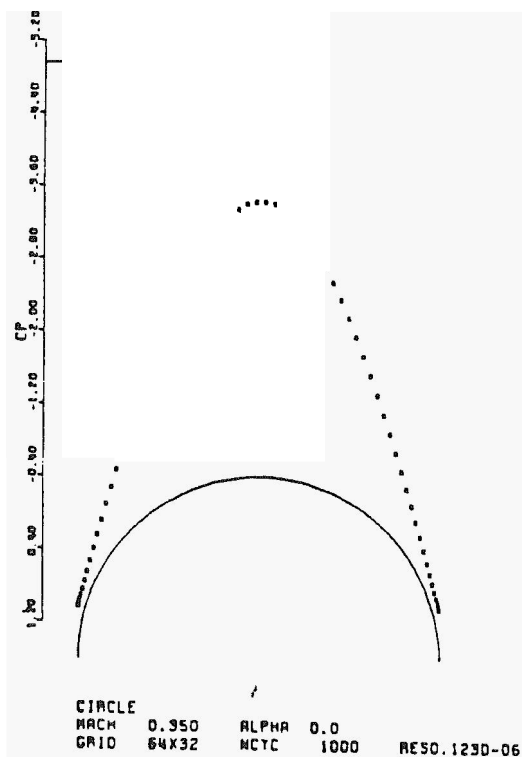
15. Gustafsson, B. and Olinger, J. "Stable Boundary Approximations for a Class of Time Discretizations of  $u_t = Au$ ", Upsala University, Dept. of Computer Sciences, Report 87, 1980.
16. Rudy, D. and Strikwerda, J. "A Non-reflecting Outflow Boundary Condition for Subsonic Navier Stokes Calculations", J. Computational Physics, Vol. 36, pp. 55-70, 1980.
17. Engquist, B. and Majda, A. "Absorbing Boundary Conditions for the Numerical Simulation of Waves", Math. Comp. Vol. 31, pp. 629-651, 1977.
18. Bayliss, A. and Turkel, E. "Outflow Boundary Conditions for Fluid Dynamics" ICASE Report 80-21, 1980.
19. Garabedian, P.R. "Estimation of the Relaxation Factor for Small Mesh Size", Math Tables Aids Comp., Vol. 10, pp. 183-185, 1956.
20. Caughey, D. and Jameson, A. "Basic Advances in the Finite Volume Method for Transonic Potential Flow Calculations", Symposium on Numerical and Physical Aspects of Aerodynamic Flows, Long Beach, 1981.
21. Steger, J. and Warming, R. "Flux Vector Splitting for the Inviscid Gas Dynamic Equations with Application to Finite Difference Methods". NASA TN 78605, 1979.
22. Roe, P.L. "The Use of the Riemann Problem in Finite Difference Schemes", Proceedings of Seventh International Conference on Numerical Methods in Fluid Dynamics, Stanford, 1980, Springer-Verlag, 1981.
23. Roe, P.L. "Numerical Algorithms for the Linear Wave Equation", Royal Aircraft Establishment Memorandum, 1980.
24. Van Leer, B. "Towards the Ultimate Conservative Differencing Scheme, V, A Second Order Sequel to Godunov's Method", J. Computational Physics, Vol. 32, pp. 101-126, 1979.



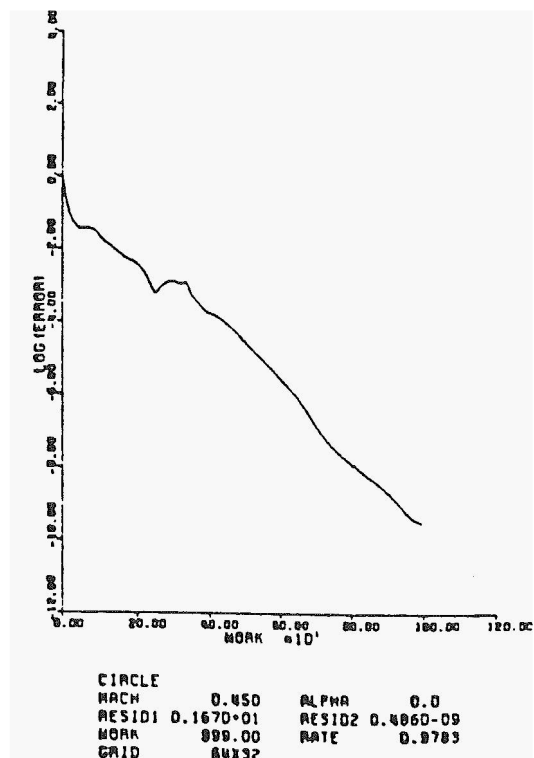
(a) Mesh



(c) Transonic flow



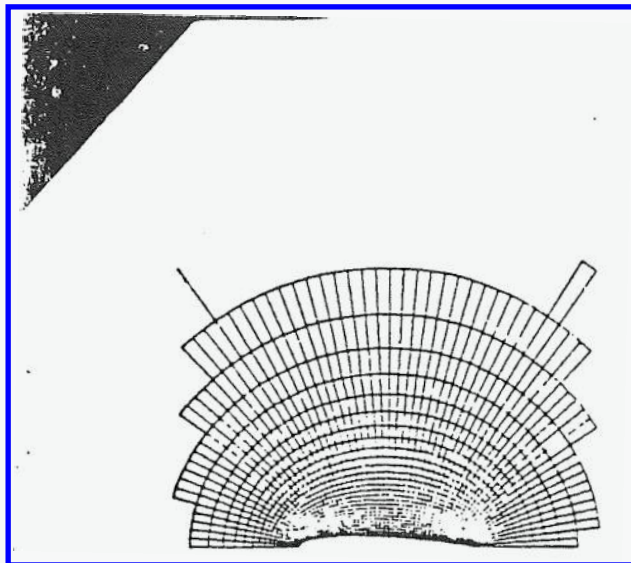
(b) Subsonic flow



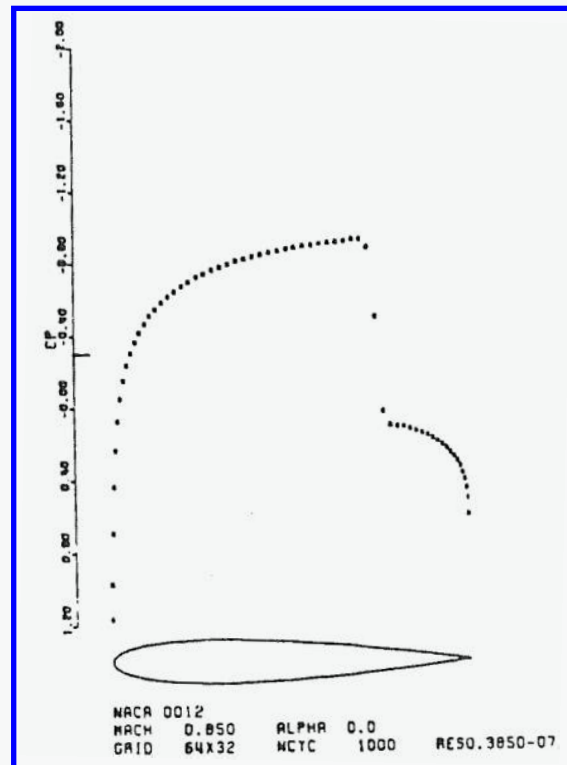
(d) Convergence history

Figure (1)

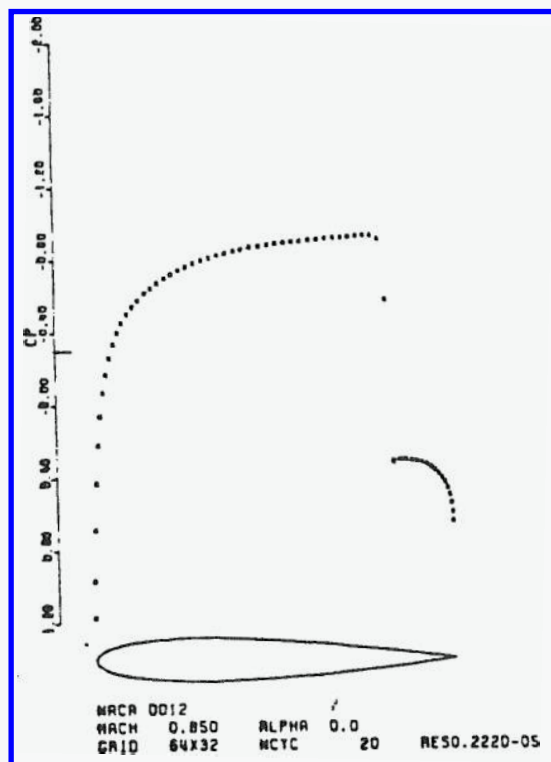
Flow past a circle.



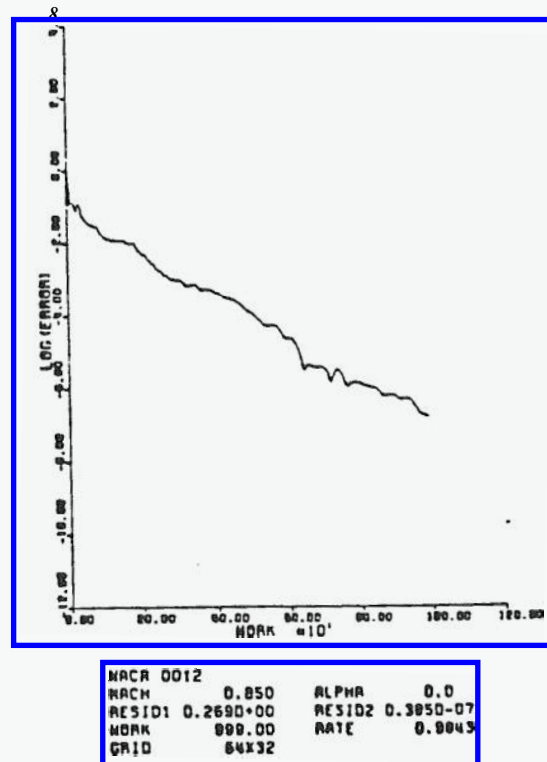
(a) Mesh



(c) Euler equations



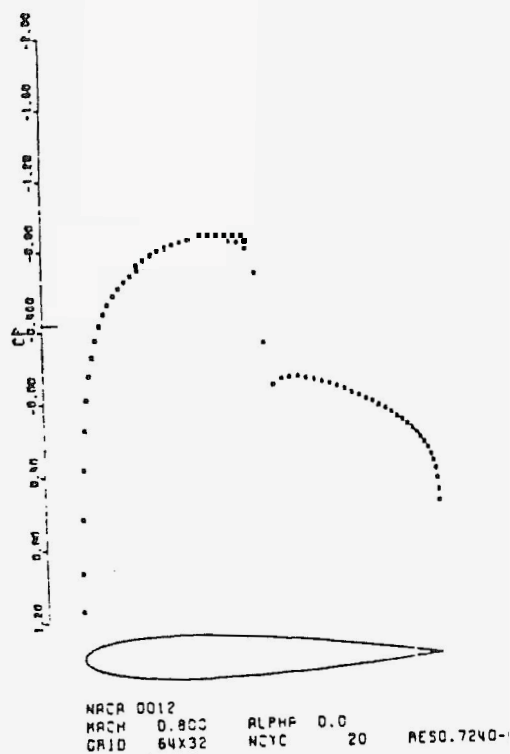
(b) Potential flow



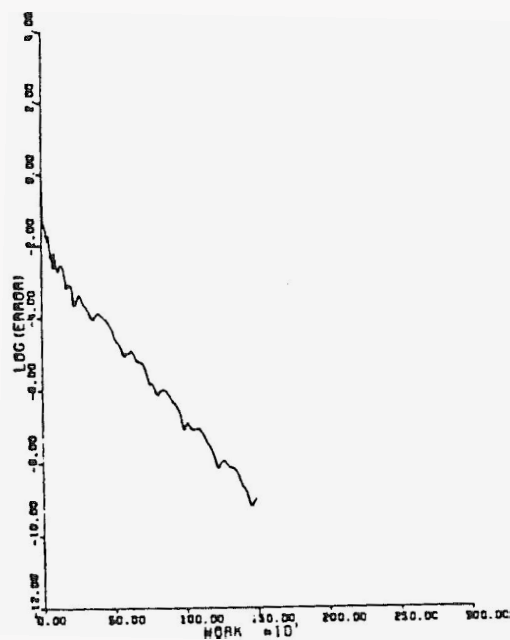
(d) Convergence history

Figure (2)  
NACA 0012 airfoil at Mach .85



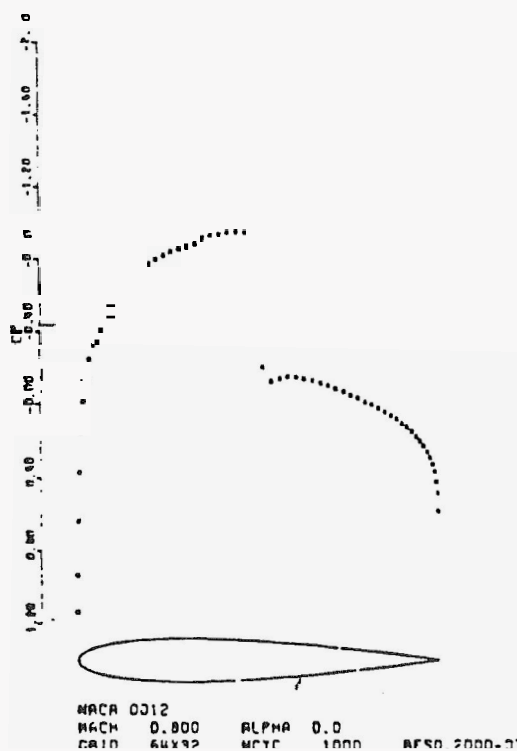


(a) Potential flow

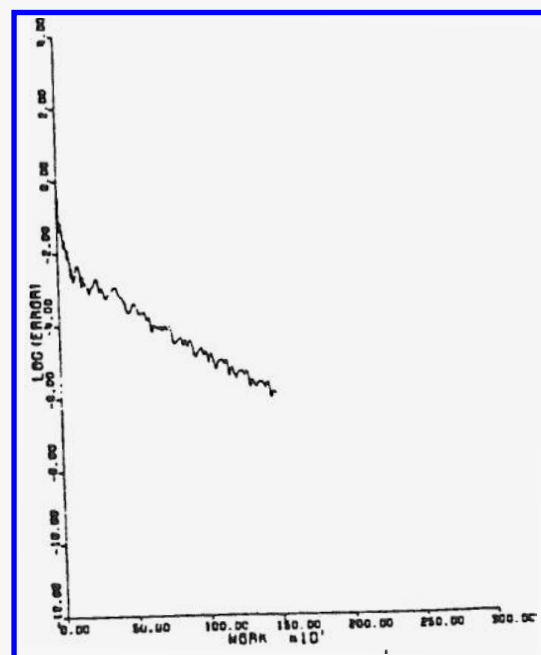


NACA 0012  
MACH 0.800 ALPHA 0.0  
RESID1 0.2330+00 RESID2 0.2400-09  
WORK 1499.00 RATE 0.9863  
GRID 64X32

(c) Convergence with enthalpy damping



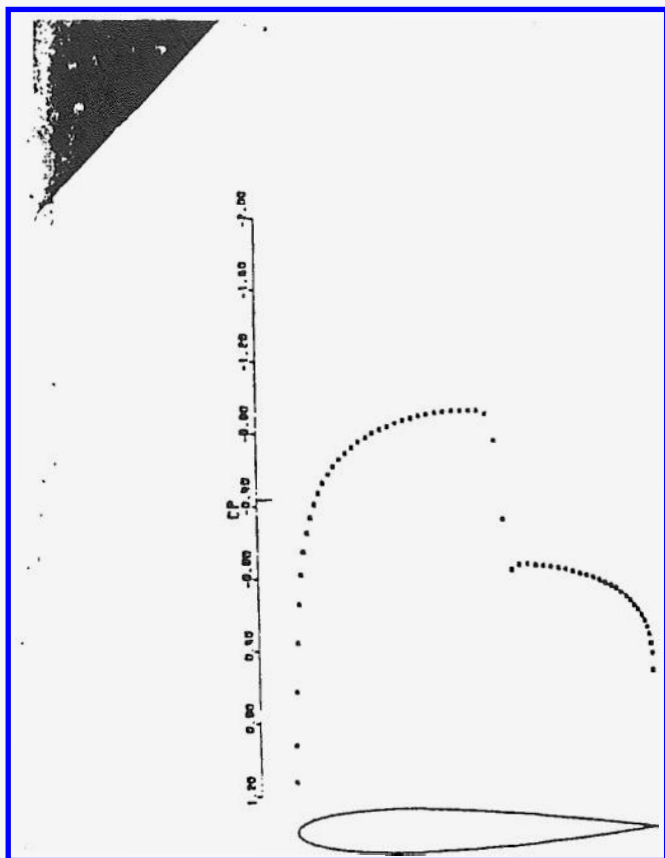
(b) Euler equations



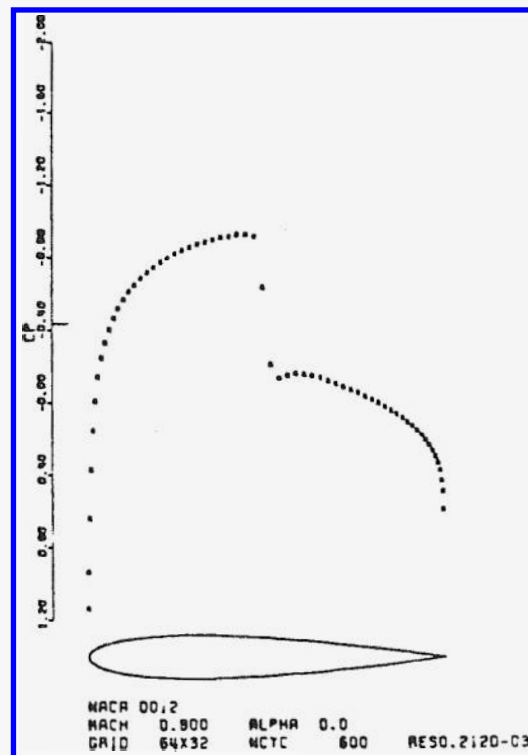
NACA 0012  
MACH 0.800 ALPHA 0.0  
RESID1 0.2390+00 RESID2 0.2690-06  
WORK 1499.00 RATE 0.9903

(d) Convergence without enthalpy d

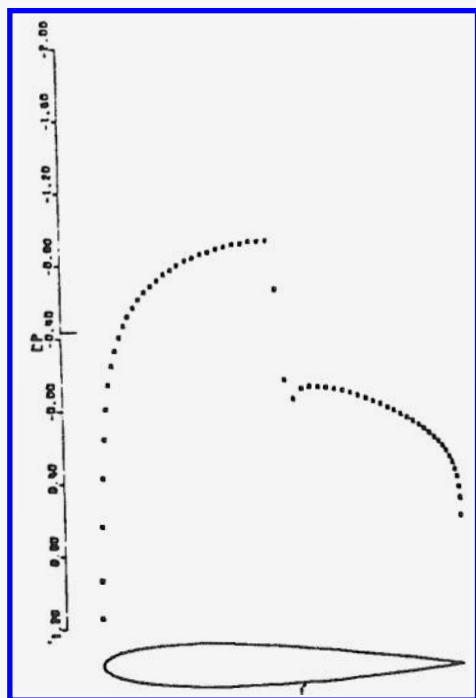
Figure 3  
NACA 0012 airfoil at Mach .80



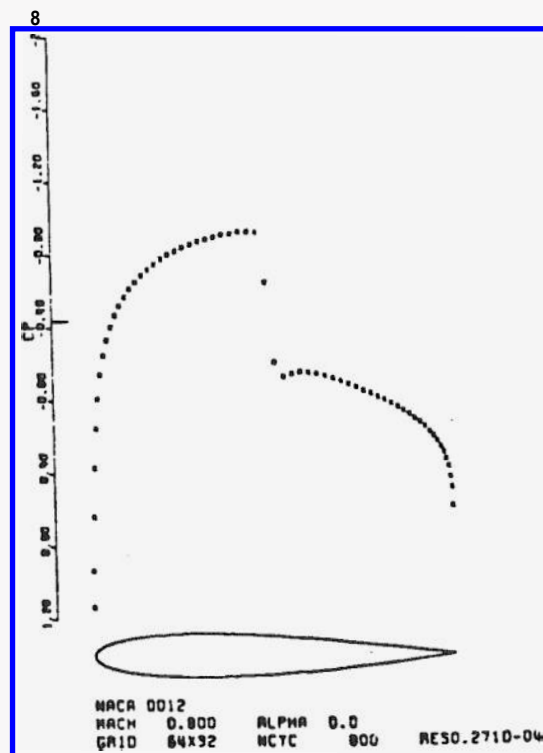
NACA 0012  
MACH 0.800 RLFHR 0.0  
GRID 64x32 NCTC 200 RESO.9370-02



NACA 0012  
MACH 0.800 ALPHA 0.0  
GRID 64x32 NCTC 600 RESO.2120-03

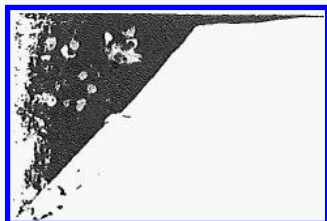


NACA 0012  
MACH 0.800 ALPHA 0.0  
GRID 64x32 NCTC 400 RESO.2580-02



NACA 0012  
MACH 0.800 ALPHA 0.0  
GRID 64x32 NCTC 800 RESO.2710-04

Figure (4)  
Development of flow field: NACA 0012 airfoil at Mach .80



I	J	R/U	U	V	H	P	PACT	S
1	1	1.3433	0.0895	0.122	0.0000	1.5109	0.1207	-0.0003
2	1	1.2950	0.2111	0.3198	0.0000	1.4336	0.3078	-0.0017
3	1	1.2160	0.3910	0.4296	0.0000	1.3130	0.4725	-0.0014
4	1	1.1369	0.5661	0.4645	0.0000	1.1953	0.6036	-0.0012
5	1	1.0695	0.7105	0.4552	0.0000	1.0976	0.7039	-0.0009
6	1	1.0140	0.8240	0.4264	0.0000	1.0192	0.7821	-0.0006
7	1	0.9693	0.0121	0.3906	0.0000	0.9570	0.8434	-0.0002
9	1	0.9328	0.9813	0.3538	0.0000	0.9072	0.8940	-0.0000
9	1	0.9025	1.0369	0.3182	0.0000	0.8663	0.9356	0.0001
10	1	0.8769	1.0825	0.2047	0.0000	0.8321	0.9711	0.0002
11	1	0.8547	1.1205	0.2537	0.0000	0.8030	1.0018	0.0003
12	1	0.8354	1.1528	0.2249	0.0000	0.7777	1.0269	0.0003
13	1	0.8181	1.1808	0.1982	0.0000	0.7553	1.0532	0.0004
14	1	0.8026	1.2054	0.1734	0.0000	0.7353	1.0753	0.0004
15	1	0.7884	1.2269	0.1501	0.0000	0.7173	1.0953	0.0005
16	1	0.7758	1.2462	0.1284	0.0000	0.7011	1.1137	0.0004
17	1	0.7640	1.2632	0.1079	0.0000	0.6864	1.1304	0.0005
18	1	0.7535	1.2786	0.0887	0.0000	0.6731	1.1461	0.0004
19	1	0.7436	1.2920	0.0705	0.0000	0.6609	1.1600	0.0000
20	1	0.7351	1.3045	0.0535	0.0000	0.6501	1.1733	0.0004
21	1	0.7267	1.3151	0.0374	0.0000	0.6400	1.1845	0.0007
22	1	0.7199	1.3252	0.0222	0.0000	0.6313	1.1961	0.0003
23	1	0.7128	1.3333	0.0030	0.0000	0.6230	1.2053	0.0005
24	1	0.7075	1.3414	-0.0054	0.0000	0.6163	1.2142	0.0001
25	1	0.7015	1.3473	-0.0179	0.0000	0.6094	1.2219	0.0009
26	1	0.6780	1.3537	-0.0293	0.0000	0.6046	1.2200	0.0000
27	1	0.6430	1.3575	-0.0406	0.0000	0.5991	1.2344	0.0011
28	1	0.6417	1.3613	-0.0512	0.0000	0.5969	1.2354	-0.0000
29	1	0.6371	1.3642	-0.0603	0.0000	0.5920	1.2434	0.0012
30	1	0.6366	1.3677	-0.0697	0.0000	0.5905	1.2481	-0.0004
31	1	0.6369	1.3619	-0.0771	0.0000	0.5922	1.2416	0.0020
32	1	0.7112	1.2239	-0.0771	0.0000	0.7134	1.0845	0.0060
33	1	0.9187	1.0204	-0.0710	0.0000	0.9087	0.8739	0.0079
34	1	0.9180	0.9872	-0.0722	0.0000	0.9466	0.8416	0.0051
35	1	0.9125	0.9945	-0.0763	0.0000	0.9391	0.8490	0.0052
36	1	0.9185	0.9994	-0.0805	0.0000	0.9337	0.8541	0.0054
37	1	0.9195	0.9976	-0.0840	-0.0000	0.9351	0.8526	0.0054
38	1	0.9127	0.9929	-0.0870	-0.0000	0.9354	0.8483	0.0054
39	1	0.9164	0.9871	-0.0898	-0.0000	0.9446	0.8430	0.0054
40	1	0.9107	0.9807	-0.0923	-0.0000	0.9505	0.8369	0.0054
41	1	0.9154	0.9734	-0.0946	-0.0000	0.9571	0.8301	0.0054
42	1	0.9106	0.9656	-0.0966	-0.0000	0.9648	0.8229	0.0054
43	1	0.9159	0.9575	-0.0984	-0.0000	0.9717	0.8153	0.0054
44	1	0.9115	0.9490	-0.1001	-0.0000	0.9794	0.8074	0.0054
45	1	0.9171	0.9403	-0.1016	-0.0000	0.9874	0.7992	0.0054
46	1	0.9130	0.9313	-0.1030	-0.0000	0.9955	0.7903	0.0055
47	1	0.9189	0.9221	-0.1042	-0.0000	1.0039	0.7824	0.0054
48	1	1.0050	0.9127	-0.1054	-0.0000	1.0125	0.7736	0.0054
49	1	1.0113	0.9029	-0.1063	-0.0000	1.0213	0.7645	0.0054
50	1	1.0177	0.8928	-0.1071	-0.0000	1.0304	0.7552	0.0054
51	1	1.0243	0.8823	-0.1077	-0.0000	1.0398	0.7456	0.0054
52	1	1.0312	0.8715	-0.1081	-0.0000	1.0496	0.7357	0.0054
53	1	1.0382	0.8602	-0.1084	-0.0000	1.0596	0.7253	0.0054
54	1	1.0456	0.8483	-0.1085	-0.0000	1.0702	0.7144	0.0054
55	1	1.0533	0.8357	-0.1082	-0.0000	1.0813	0.7029	0.0054
56	1	1.0615	0.8225	-0.1077	-0.0000	1.0931	0.6909	0.0054
57	1	1.0701	0.8082	-0.1069	-0.0000	1.1054	0.6779	0.0054
58	1	1.0795	0.7928	-0.1058	-0.0000	1.1190	0.6639	0.0054
59	1	1.0895	0.7756	-0.1039	-0.0006	1.1336	0.6484	0.0055
60	1	1.1012	0.7564	-0.1015	-0.0000	1.1505	0.6310	0.0053
61	1	1.1136	0.7336	-0.0991	-0.0000	1.1689	0.6105	0.0053
62	1	1.1306	0.7063	-0.0927	-0.0000	1.1933	0.5660	0.0049
63	1	1.1489	0.6660	-0.0858	-0.0000	1.2220	0.5503	0.0046
64	1	1.1683	0.6133	-0.0667	-0.0000	1.2683	0.5032	0.0044
65	1	1.1813	0.6133	0.0667	-0.0000	1.2683	0.5032	0.0044

Figure (5)  
Printout of flow field quantities in the cells along the surface  
NACA 0012 airfoil at Mach .80

**This article has been cited by:**

1. Guangyu Shi, Qing Xiao, Qiang Zhu. 2020. Numerical Investigation of an Actively and Passively Controlled Skeleton-Reinforced Caudal Fin. *AIJA Journal* **58**:11, 4644-4658. [[Abstract](#)] [[Full Text](#)] [[PDF](#)] [[PDF Plus](#)]
2. Charles A. Mader, Gaetan K. W. Kenway, Anil Yildirim, Joaquim R. R. A. Martins. 2020. ADflow: An Open-Source Computational Fluid Dynamics Solver for Aerodynamic and Multidisciplinary Optimization. *Journal of Aerospace Information Systems* **17**:9, 508-527. [[Abstract](#)] [[Full Text](#)] [[PDF](#)] [[PDF Plus](#)]
3. Caleb J. Barnes, Miguel R. Visbal. 2020. Angle of Attack and Core Size Effects on Transitional Vortical-Gust-Airfoil Interactions. *AIJA Journal* **58**:7, 2881-2898. [[Abstract](#)] [[Full Text](#)] [[PDF](#)] [[PDF Plus](#)]
4. Tushar R. Phadnis, P. Raveendranath, T. Jayachandran. 2020. Effect of Ply Orientation on the In-Depth Response of Carbon-Phenolic Ablative. *Journal of Thermophysics and Heat Transfer* **34**:3, 650-658. [[Abstract](#)] [[Full Text](#)] [[PDF](#)] [[PDF Plus](#)]
5. Laurence Kedward, Christian B. Allen. Implementation of a Highly-Parallel Finite Volume Test Bench Code in OpenCL . [[Abstract](#)] [[PDF](#)] [[PDF Plus](#)]
6. Christian Perron, Dushhyanth Rajaram, Dimitri Mavris. Development of a Multi-Fidelity Reduced-Order Model Based on Manifold Alignment . [[Abstract](#)] [[PDF](#)] [[PDF Plus](#)]
7. Lin Zhou, Jiangtao Huang, Zhenghong Gao, Wei Zhang. 2020. Three-Dimensional Aerodynamic/Stealth Optimization Based on Adjoint Sensitivity Analysis for Scattering Problem. *AIJA Journal* **58**:6, 2702-2715. [[Abstract](#)] [[Full Text](#)] [[PDF](#)] [[PDF Plus](#)]
8. Roberto F. Bobenrieth Miserda, Braulio Gutierrez Pimenta, Luiza Sampaio da Rocha. 2020. Numerical Simulation of Rotor-Stator Interaction Noise in Transonic Cascades. *Journal of Propulsion and Power* **36**:3, 363-380. [[Abstract](#)] [[Full Text](#)] [[PDF](#)] [[PDF Plus](#)]
9. Anand Amrit, Leifur Leifsson, Slawomir Koziel. 2020. Fast Multi-Objective Aerodynamic Optimization Using Sequential Domain Patching and Multifidelity Models. *Journal of Aircraft* **57**:3, 388-398. [[Abstract](#)] [[Full Text](#)] [[PDF](#)] [[PDF Plus](#)]
10. Anastasios S. Lyrintzis, Marco Coderoni. 2020. Overview of the Use of Large-Eddy Simulations in Jet Aeroacoustics. *AIJA Journal* **58**:4, 1620-1638. [[Abstract](#)] [[Full Text](#)] [[PDF](#)] [[PDF Plus](#)]
11. Roberto Paoli, Adèle Poubeau, Daniel Cariolle. 2020. Large-Eddy Simulations of a Reactive Solid Rocket Motor Plume. *AIJA Journal* **58**:4, 1639-1656. [[Abstract](#)] [[Full Text](#)] [[PDF](#)] [[PDF Plus](#)]
12. Thomas D. Economou. 2020. Simulation and Adjoint-Based Design for Variable Density Incompressible Flows with Heat Transfer. *AIJA Journal* **58**:2, 757-769. [[Abstract](#)] [[Full Text](#)] [[PDF](#)] [[PDF Plus](#)]
13. Nikhil Nigam, Sritharan K. Ayyalasomayajula, Yuye Tang, Padmanabha Ketha, Victorien Menier, Rick W. Fenrich, Juan J. Alonso. Aero-structural Design Tool for Advanced Exhaust Systems . [[Abstract](#)] [[PDF](#)] [[PDF Plus](#)]
14. Daniel J. Poole, Christian B. Allen, T. Rendall. Efficient Modal Design Variables for Optimization of Aero-Elastic Wing . [[Abstract](#)] [[PDF](#)] [[PDF Plus](#)]
15. Rachit Prasad, Seongim Choi. Aerodynamic Shape Optimization for Flutter/LCO based design using Coupled Adjoint . [[Abstract](#)] [[PDF](#)] [[PDF Plus](#)]
16. Jethro Nagawkar, Leifur T. Leifsson, Xiaosong Du. Applications of Polynomial Chaos-Based Cokriging to Aerodynamic Design Optimization Benchmark Problems . [[Abstract](#)] [[PDF](#)] [[PDF Plus](#)]
17. Laurence Kedward, Christian B. Allen, T. Rendall. Comparing Matrix-based and Matrix-free Discrete Adjoint Approaches to the Euler Equations . [[Abstract](#)] [[PDF](#)] [[PDF Plus](#)]
18. Xiaosong Du, Ping He, Joaquim Martins. A B-Spline-based Generative Adversarial Network Model for Fast Interactive Airfoil Aerodynamic Optimization . [[Abstract](#)] [[PDF](#)] [[PDF Plus](#)]
19. . Modeling and Simulations of High-Pressure Practical Flows 631-677. [[Citation](#)] [[Full Text](#)] [[PDF](#)] [[PDF Plus](#)]
20. Tuan M. Nguyen, William A. Sirignano. 2019. Spontaneous and Triggered Longitudinal Combustion Instability in a Single-Injector Liquid-Rocket Combustor. *AIJA Journal* **57**:12, 5351-5364. [[Abstract](#)] [[Full Text](#)] [[PDF](#)] [[PDF Plus](#)]
21. Jieyun Pan, Feng Liu. 2019. Wing Flutter Prediction by a Small-Disturbance Euler Method on Body-Fitted Curvilinear Grids. *AIJA Journal* **57**:11, 4873-4884. [[Abstract](#)] [[Full Text](#)] [[PDF](#)] [[PDF Plus](#)]
22. Hang Li, Kivanc Ekici. 2019. Aeroelastic Modeling of the AGARD 445.6 Wing Using the Harmonic-Balance-Based One-Shot Method. *AIJA Journal* **57**:11, 4885-4902. [[Abstract](#)] [[Full Text](#)] [[PDF](#)] [[PDF Plus](#)]
23. Carlos Lozano. 2019. Watch Your Adjoints! Lack of Mesh Convergence in Inviscid Adjoint Solutions. *AIJA Journal* **57**:9, 3991-4006. [[Abstract](#)] [[Full Text](#)] [[PDF](#)] [[PDF Plus](#)]
24. Daniel J. Garmann, Miguel R. Visbal. 2019. High-Fidelity Simulations of Afterbody Vortex Flows. *AIJA Journal* **57**:9, 3980-3990. [[Abstract](#)] [[Full Text](#)] [[PDF](#)] [[PDF Plus](#)]



25. Gunther Wilke. 2019. Variable-Fidelity Methodology for the Aerodynamic Optimization of Helicopter Rotors. *AIAA Journal* 57:8, 3145-3158. [[Abstract](#)] [[Full Text](#)] [[PDF](#)] [[PDF Plus](#)]
26. Romain Gojon, Ephraim Gutmark, Mihai Mihaescu. 2019. Antisymmetric Oscillation Modes in Rectangular Screeching Jets. *AIAA Journal* 57:8, 3422-3441. [[Abstract](#)] [[Full Text](#)] [[PDF](#)] [[PDF Plus](#)]
27. Patrick R. Hammer, David A. Olson, Miguel R. Visbal, Ahmed M. Naguib, Manoochehr M. Koochesfahani. 2019. Joint Computational-Experimental Investigation of Harmonically Pitching Airfoil Aerodynamics in Uniform-Shear Approach Flow. *AIAA Journal* 57:8, 3290-3298. [[Abstract](#)] [[Full Text](#)] [[PDF](#)] [[PDF Plus](#)]
28. Xavier Bertrand, Frédéric Tost, Steeve Champagneux. Wing Airfoil Pressure Calibration with Deep Learning . [[Citation](#)] [[PDF](#)] [[PDF Plus](#)]
29. Laurence Kedward, Christian B. Allen, T. Rendall. Application of Subdivision Surfaces to Aerodynamic Wing Shape Optimisation . [[Citation](#)] [[PDF](#)] [[PDF Plus](#)]
30. Zhenming Xu, Zhonghua Han, Zhen Zhu, Wenping Song. On the Flow Mechanism of Forward Swept Natural-Laminar-Flow Wing for Crossflow Instability Suppression . [[Citation](#)] [[PDF](#)] [[PDF Plus](#)]
31. David Quero. An input-independent method for solving weakly nonlinear partial differential equations in the frequency domain: application to the Euler equations . [[Citation](#)] [[PDF](#)] [[PDF Plus](#)]
32. Aslihan Vuruskan, Serhat Hosder. 2019. Impact of Turbulence Models and Shape Parameterization on Robust Aerodynamic Shape Optimization. *Journal of Aircraft* 56:3, 1099-1115. [[Abstract](#)] [[Full Text](#)] [[PDF](#)] [[PDF Plus](#)]
33. Bernhard Semlitsch, Daniel R. Cuppoletti, Ephraim J. Gutmark, Mihai Mihaescu. 2019. Transforming the Shock Pattern of Supersonic Jets Using Fluidic Injection. *AIAA Journal* 57:5, 1851-1861. [[Abstract](#)] [[Full Text](#)] [[PDF](#)] [[PDF Plus](#)]
34. P. Bekemeyer, M. Ripepi, R. Heinrich, S. Görtz. 2019. Nonlinear Unsteady Reduced-Order Modeling for Gust-Load Predictions. *AIAA Journal* 57:5, 1839-1850. [[Abstract](#)] [[Full Text](#)] [[PDF](#)] [[PDF Plus](#)]
35. Anastasios S. Lyrintzis, Marco Coderoni. The Use of Large Eddy Simulations in Jet Aeroacoustics . [[Citation](#)] [[PDF](#)] [[PDF Plus](#)]
36. Ross Higgins, Antonio Jimenez-Garcia, George N. Barakos, Nicholas Bown. A Time-Marching Aeroelastic Method Applied to Propeller Flutter . [[Citation](#)] [[PDF](#)] [[PDF Plus](#)]
37. Kevin R. Holst, Ryan S. Glasby, Jon T. Erwin, Douglas L. Stefanski, James G. Coder. High-Order Shock Capturing Techniques using HPCMP CREATE-AV Kestrel . [[Citation](#)] [[PDF](#)] [[PDF Plus](#)]
38. William C. Tyson, Charles W. Jackson, Christopher J. Roy. BlueRidge: A Higher-Order Finite-Volume Solver . [[Citation](#)] [[PDF](#)] [[PDF Plus](#)]
39. Jiang-Bo Chi, Zhong-Hua Han, Tian-Lun Fan, Zhen Zhu, Wen-Ping Song. Hybrid Inverse/Optimization Design Approach for Transonic Natural-Laminar-Flow Airfoils . [[Citation](#)] [[PDF](#)] [[PDF Plus](#)]
40. Rayomand Gundevia, Feng Liu. Resonance Prediction and the Limitations for Linear Methods . [[Citation](#)] [[PDF](#)] [[PDF Plus](#)]
41. Rayomand Gundevia, Feng Liu. On the Accuracy of Harmonic Methods and a New Similarity Rule for Unsteady Transonic Flow . [[Citation](#)] [[PDF](#)] [[PDF Plus](#)]
42. Daniel J. Poole, Christian B. Allen, T. Rendall. Efficient Aero-Structural Wing Optimization Using Compact Aerofoil Decomposition . [[Citation](#)] [[PDF](#)] [[PDF Plus](#)]
43. Alexandros Kontogiannis, Matthieu Parenteau, Eric Laurendeau. Viscous-Inviscid Analysis of Transonic Swept Wings using 2.5D RANS and Parametric Shapes . [[Citation](#)] [[PDF](#)] [[PDF Plus](#)]
44. Michael Piotrowski, David W. Zingg. Investigation of a Local Correlation-based Transition Model in a Newton-Krylov Algorithm . [[Citation](#)] [[PDF](#)] [[PDF Plus](#)]
45. Charles W. Jackson, William C. Tyson, Christopher J. Roy. Turbulence Model Implementation and Verification in the SENSEI CFD Code . [[Citation](#)] [[PDF](#)] [[PDF Plus](#)]
46. Yingxiu Chen, Anping Hou, Weiwei Wang, Mingming Zhang. 2018. Performance Estimation Method for Nonuniform Tip Clearance Cases. *Journal of Propulsion and Power* 34:6, 1355-1363. [[Abstract](#)] [[Full Text](#)] [[PDF](#)] [[PDF Plus](#)]
47. F. Falissard, R. Boisard, R. Gaveriaux, G. Delattre, P. Gardarein, A. Chelius, S. Canard-Caruana, Y. Mauffrey. 2018. Influence of Blade Deformations on Open-Rotor Low-Speed and High-Speed Aerodynamics and Aeroacoustics. *Journal of Aircraft* 55:6, 2267-2281. [[Abstract](#)] [[Full Text](#)] [[PDF](#)] [[PDF Plus](#)]
48. Carlos Lozano. 2018. Singular and Discontinuous Solutions of the Adjoint Euler Equations. *AIAA Journal* 56:11, 4437-4452. [[Abstract](#)] [[Full Text](#)] [[PDF](#)] [[PDF Plus](#)]
49. Lei Zhan, Juntao Xiong, Feng Liu, Zuoli Xiao. 2018. Fully Implicit Chebyshev Time-Spectral Method for General Unsteady Flows. *AIAA Journal* 56:11, 4474-4486. [[Abstract](#)] [[Full Text](#)] [[PDF](#)] [[PDF Plus](#)]

50. Caleb J. Barnes, Miguel R. Visbal. 2018. Clockwise Vortical-Gust/Airfoil Interactions at a Transitional Reynolds Number. *ALAA Journal* 56:10, 3863-3874. [[Abstract](#)] [[Full Text](#)] [[PDF](#)] [[PDF Plus](#)]
51. Boping Ma, Gang Wang, Jiong Ren, Zhengyin Ye, Zhijin Lei, Gecheng Zha. 2018. Near-Field Sonic-Boom Prediction and Analysis with Hybrid Grid Navier–Stokes Solver. *Journal of Aircraft* 55:5, 1890-1904. [[Abstract](#)] [[Full Text](#)] [[PDF](#)] [[PDF Plus](#)]
52. Romain Dupuis, Jean-Christophe Jouhaud, Pierre Sagaut. 2018. Surrogate Modeling of Aerodynamic Simulations for Multiple Operating Conditions Using Machine Learning. *ALAA Journal* 56:9, 3622-3635. [[Abstract](#)] [[Full Text](#)] [[PDF](#)] [[PDF Plus](#)] [[Supplementary Material](#)]
53. Yachao Lee, Wei Yao, Xuejun Fan. 2018. Low-Dissipative Hybrid Compressible Solver Designed for Large-Eddy Simulation of Supersonic Turbulent Flows. *ALAA Journal* 56:8, 3086-3096. [[Abstract](#)] [[Full Text](#)] [[PDF](#)] [[PDF Plus](#)]
54. Hang Li, Kivanc Ekici. 2018. Improved One-Shot Approach for Modeling Viscous Transonic Limit Cycle Oscillations. *ALAA Journal* 56:8, 3138-3152. [[Abstract](#)] [[Full Text](#)] [[PDF](#)] [[PDF Plus](#)]
55. Tuan M. Nguyen, William A. Sirignano. Spontaneous and Triggered Longitudinal Combustion Instability in a Single-Injector Rocket Engine . [[Citation](#)] [[PDF](#)] [[PDF Plus](#)]
56. Takayasu Fujino, Daiki Ichinokiyama, Takuma Ichikawa. 2018. Plasma Characteristics and Performance of Nonequilibrium Disk Magnetohydrodynamic Generator with Swirl Vanes. *Journal of Propulsion and Power* 34:4, 992-1001. [[Abstract](#)] [[Full Text](#)] [[PDF](#)] [[PDF Plus](#)]
57. David Hue, Quentin Chanzy, Sâm Landier. 2018. DPW-6: Drag Analyses and Increments Using Different Geometries of the Common Research Model Airliner. *Journal of Aircraft* 55:4, 1509-1521. [[Abstract](#)] [[Full Text](#)] [[PDF](#)] [[PDF Plus](#)]
58. Dmitry Kolomenskiy, Roberto Paoli. 2018. Numerical Simulation of the Wake of an Airliner. *Journal of Aircraft* 55:4, 1689-1699. [[Abstract](#)] [[Full Text](#)] [[PDF](#)] [[PDF Plus](#)] [[Supplementary Material](#)]
59. Aurelia Cartieri, David Hue, Quentin Chanzy, Olivier Atinault. 2018. Experimental Investigations on Common Research Model at ONERA-S1MA–Drag Prediction Workshop Numerical Results. *Journal of Aircraft* 55:4, 1491-1508. [[Abstract](#)] [[Full Text](#)] [[PDF](#)] [[PDF Plus](#)]
60. Stefan Keye, Dimitri Mavriplis. 2018. Summary of Case 5 from Sixth Drag Prediction Workshop: Coupled Aerostructural Simulation. *Journal of Aircraft* 55:4, 1380-1387. [[Abstract](#)] [[Full Text](#)] [[PDF](#)] [[PDF Plus](#)]
61. James G. Coder, David Hue, Gaetan Kenway, Thomas H. Pulliam, Anthony J. Sclafani, Leonel Serrano, John C. Vassberg. 2018. Contributions to the Sixth Drag Prediction Workshop Using Structured, Overset Grid Methods. *Journal of Aircraft* 55:4, 1406-1419. [[Abstract](#)] [[Full Text](#)] [[PDF](#)] [[PDF Plus](#)]
62. D. J. Poole, C. B. Allen, T. C. S. Rendall. 2018. Global Optimization of Wing Aerodynamic Optimization Case Exhibiting Multimodality. *Journal of Aircraft* 55:4, 1576-1591. [[Abstract](#)] [[Full Text](#)] [[PDF](#)] [[PDF Plus](#)]
63. Zhong-Hua Han, Jing Chen, Ke-Shi Zhang, Zhen-Ming Xu, Zhen Zhu, Wen-Ping Song. 2018. Aerodynamic Shape Optimization of Natural-Laminar-Flow Wing Using Surrogate-Based Approach. *ALAA Journal* 56:7, 2579-2593. [[Abstract](#)] [[Full Text](#)] [[PDF](#)] [[PDF Plus](#)]
64. Andrea Da Ronch, Jernjej Drofelnik, Michel van Rooij, Marco Panzeri, Roberto d'Ippolito. On Uncertainty Quantification of the Flow Predictions around the NATO STO AVT-251 Unmanned Combat Aerial Vehicle . [[Citation](#)] [[PDF](#)] [[PDF Plus](#)]
65. Daniel Kharlamov, Jernjej Drofelnik, Andrea Da Ronch, Scott Walker. Rapid Load Calculations Using an Efficient Unsteady Aerodynamic Solver . [[Citation](#)] [[PDF](#)] [[PDF Plus](#)]
66. Jangho Park, Seongim Choi, Pradeep Raj. Multi-response Gaussian Process Regression for Multidisciplinary Design Analysis and Optimization . [[Citation](#)] [[PDF](#)] [[PDF Plus](#)]
67. Wrik Mallik, Joseph A. Schetz, Rakesh K. Kapania. 2018. Rapid Transonic Flutter Analysis for Aircraft Conceptual Design Applications. *ALAA Journal* 56:6, 2389-2402. [[Abstract](#)] [[Full Text](#)] [[PDF](#)] [[PDF Plus](#)]
68. Daniel Destarac, Gérald Carrier, George R. Anderson, Siva Nadarajah, Daniel J. Poole, John C. Vassberg, David W. Zingg. 2018. Example of a Pitfall in Aerodynamic Shape Optimization. *ALAA Journal* 56:4, 1532-1540. [[Abstract](#)] [[Full Text](#)] [[PDF](#)] [[PDF Plus](#)]
69. Tuan M. Nguyen, Pavel P. Popov, William A. Sirignano. 2018. Longitudinal Combustion Instability in a Rocket Engine with a Single Coaxial Injector. *Journal of Propulsion and Power* 34:2, 354-373. [[Abstract](#)] [[Full Text](#)] [[PDF](#)] [[PDF Plus](#)]
70. He-Yong Xu, Chen-Liang Qiao, Hui-Qiang Yang, Zheng-Yin Ye. 2018. Active Circulation Control on the Blunt Trailing Edge Wind Turbine Airfoil. *ALAA Journal* 56:2, 554-570. [[Abstract](#)] [[Full Text](#)] [[PDF](#)] [[PDF Plus](#)]
71. Rachit Prasad, Hyunsoon Kim, Seongim Choi. Flutter Related Design Optimization using the Time Spectral and Coupled Adjoint Method . [[Citation](#)] [[PDF](#)] [[PDF Plus](#)]
72. Rachit Prasad, Hyunsoon Kim, Seongim Choi, Seulgi Yi. High Fidelity Prediction of Flutter/LCO using Time Spectral Method . [[Citation](#)] [[PDF](#)] [[PDF Plus](#)]

73. Jieyun Pan, Feng Liu. Wing Flutter Prediction by a Small-Disturbance Euler (SD-Euler) Method on Body-fitted Curvilinear Grid . [\[Citation\]](#) [\[PDF\]](#) [\[PDF Plus\]](#)
74. Sirko Bartholomay, Grigoris Michos, Sebastian Perez-Becker, George Pechlivanoglou, Christian Nayeri, Grigoris Nikolaouk, Christian O. Paschereit. Towards Active Flow Control on a Research Scale Wind Turbine Using PID controlled Trailing Edge Flaps . [\[Citation\]](#) [\[PDF\]](#) [\[PDF Plus\]](#)
75. Thomas Reist, David W. Zingg. Application of Diablo to Three-Dimensional Benchmark Problems for Reynolds-Averaged Navier-Stokes Solvers . [\[Citation\]](#) [\[PDF\]](#) [\[PDF Plus\]](#)
76. Leonardo M. Carvalho, Alexandre C. Almeida, Ricardo G. da Silva, Edson Basso, Joao Luiz F. Azevedo. Robust Parallel Computations of Turbulent Aerodynamic Flows . [\[Citation\]](#) [\[PDF\]](#) [\[PDF Plus\]](#)
77. Romain Dupuis, Jean-Christophe Jouhaud, Pierre Sagaut. Aerodynamic Data Predictions for Transonic Flows via a Machine-Learning-based Surrogate Model . [\[Citation\]](#) [\[PDF\]](#) [\[PDF Plus\]](#)
78. Anand Amrit, Leifur T. Leifsson, Slawomir Koziel. Aerodynamic Design Exploration through Point-By-Point Pareto Set Identification using Local Surrogate Models . [\[Citation\]](#) [\[PDF\]](#) [\[PDF Plus\]](#)
79. G. J. M. Loupy, G. N. Barakos, N. J. Taylor. 2018. Cavity Flow over a Transonic Weapons Bay During Door Operation. *Journal of Aircraft* **55**:1, 339-354. [\[Abstract\]](#) [\[Full Text\]](#) [\[PDF\]](#) [\[PDF Plus\]](#)
80. David Koo, David W. Zingg. 2018. Investigation into Aerodynamic Shape Optimization of Planar and Nonplanar Wings. *AIAA Journal* **56**:1, 250-263. [\[Abstract\]](#) [\[Full Text\]](#) [\[PDF\]](#) [\[PDF Plus\]](#)
81. David Hue, Olivier Vermeersch, J  r  my Duchemin, Olivier Colin, Dac Tran. 2018. Wind-Tunnel and CFD Investigations Focused on Transition and Performance Predictions of Laminar Wings. *AIAA Journal* **56**:1, 132-145. [\[Abstract\]](#) [\[Full Text\]](#) [\[PDF\]](#) [\[PDF Plus\]](#)
82. Pierre-Olivier Tardif, Siva Nadarajah. 2017. Three-Dimensional Aeroelastic Solutions via the Nonlinear Frequency-Domain Method. *AIAA Journal* **55**:10, 3553-3569. [\[Abstract\]](#) [\[Full Text\]](#) [\[PDF\]](#) [\[PDF Plus\]](#)
83. A. C. L. M. van Rooij, J. Nitzsche, R. P. Dwight. 2017. Prediction of Aeroelastic Limit-Cycle Oscillations Based on Harmonic Forced-Motion Oscillations. *AIAA Journal* **55**:10, 3517-3529. [\[Abstract\]](#) [\[Full Text\]](#) [\[PDF\]](#) [\[PDF Plus\]](#)
84. Reza Djeddi, Andrew Kaminsky, Kivanc Ekici. 2017. Convergence Acceleration of Fluid Dynamics Solvers Using a Reduced-Order Model. *AIAA Journal* **55**:9, 3059-3071. [\[Abstract\]](#) [\[Full Text\]](#) [\[PDF\]](#) [\[PDF Plus\]](#)
85. Matthew V. Fischels, R. G. Rajagopalan. 2017. Family of Runge-Kutta-Based Algorithms for Unsteady Incompressible Flows. *AIAA Journal* **55**:8, 2630-2644. [\[Abstract\]](#) [\[Full Text\]](#) [\[PDF\]](#) [\[PDF Plus\]](#)
86. Jonas Verri  re, Fabien Gand, S  bastien Deck. 2017. Zonal Detached Eddy Simulations of a Dual-Stream Jet: Turbulence Rate Sensitivity. *AIAA Journal* **55**:8, 2503-2521. [\[Abstract\]](#) [\[Full Text\]](#) [\[PDF\]](#) [\[PDF Plus\]](#)
87. Daniel J. Garmann, Miguel R. Visbal. 2017. Analysis of Tip Vortex Near-Wake Evolution for Stationary and Oscillating Wings. *AIAA Journal* **55**:8, 2686-2702. [\[Abstract\]](#) [\[Full Text\]](#) [\[PDF\]](#) [\[PDF Plus\]](#)
88. Philipp Bekemeyer, Reik Thormann, Sebastian Timme. 2017. Frequency-Domain Gust Response Simulation Using Computational Fluid Dynamics. *AIAA Journal* **55**:7, 2174-2185. [\[Abstract\]](#) [\[Full Text\]](#) [\[PDF\]](#) [\[PDF Plus\]](#)
89. Gaetan Loupy, George N. Barakos. Modelling of Transonic Shallow Cavity Flows . [\[Citation\]](#) [\[PDF\]](#) [\[PDF Plus\]](#)
90. Slawomir Koziel, Leifur T. Leifsson. Statistical-Analysis-Based Setup of Physics-based Surrogates and Optimization Process Resolution for Variable-Fidelity Aerodynamic Design . [\[Citation\]](#) [\[PDF\]](#) [\[PDF Plus\]](#)
91. Anand Amrit, Xiaosong Du, Andrew S. Thelen, Leifur T. Leifsson, Slawomir Koziel. Aerodynamic Design of the RAE 2822 in Transonic Viscous Flow: Single- and Multi-point Optimization Studies . [\[Citation\]](#) [\[PDF\]](#) [\[PDF Plus\]](#)
92. Freddie D. Witherden, Antony Jameson. Future Directions in Computational Fluid Dynamics . [\[Citation\]](#) [\[PDF\]](#) [\[PDF Plus\]](#)
93. Julien Marty, Rapha  l Barrier, Eric Garnier. Impact of distortions due to separation in S-duct inlet on compressor stage behavior and performances . [\[Citation\]](#) [\[PDF\]](#) [\[PDF Plus\]](#)
94. Yann Mauffrey, Arnaud Geeraert, Simon Verley. Comparison Between Coupled CFD/CSM Hot Shape Prediction and AIPX-7 CROR Experimental Data . [\[Citation\]](#) [\[PDF\]](#) [\[PDF Plus\]](#)
95. Philipp Bekemeyer, Sebastian Timme. Reduced Order Transonic Aeroelastic Gust Response Simulation of Large Aircraft . [\[Citation\]](#) [\[PDF\]](#) [\[PDF Plus\]](#)
96. Daniel J. Poole, Christian B. Allen, T. Rendall. Global Optimization of Multimodal Aerodynamic Optimization Benchmark Case . [\[Citation\]](#) [\[PDF\]](#) [\[PDF Plus\]](#)
97. Carlos Junqueira-Junior, Joao Luiz F. Azevedo, Sami Yamouni, William Wolf. Computational Performance of a LES Solver for Supersonic Jet Flow Applications . [\[Citation\]](#) [\[PDF\]](#) [\[PDF Plus\]](#)

98. Gaetan K. W. Kenway, Joaquim R. R. A. Martins. 2017. Buffet-Onset Constraint Formulation for Aerodynamic Shape Optimization. *AIAA Journal* 55:6, 1930-1947. [[Abstract](#)] [[Full Text](#)] [[PDF](#)] [[PDF Plus](#)]
99. C. De Maesschalck, C. Lacor, G. Paniagua, S. Lavagnoli, A. Remiot, L. Bricteux. 2017. Performance Robustness of Turbine Squealer Tip Designs Due to Manufacturing and Engine Operation. *Journal of Propulsion and Power* 33:3, 740-749. [[Abstract](#)] [[Full Text](#)] [[PDF](#)] [[PDF Plus](#)]
100. Antony Jameson. 2017. Origins and Further Development of the Jameson-Schmidt-Turkel Scheme. *AIAA Journal* 55:5, 1487-1510. [[Abstract](#)] [[Full Text](#)] [[PDF](#)] [[PDF Plus](#)]
101. Simon Bourgault-Côté, Shahin Ghasemi, Ali Mosahebi, Éric Laurendeau. 2017. Extension of a Two-Dimensional Navier-Stokes Solver for Infinite Swept Flow. *AIAA Journal* 55:2, 662-667. [[Citation](#)] [[Full Text](#)] [[PDF](#)] [[PDF Plus](#)]
102. Sami Yamouni, Carlos Junqueira-Junior, Joao Luiz F. Azevedo, William R. Wolf. Dynamic Mode Decomposition of High Reynolds Number Supersonic Jet Flows . [[Citation](#)] [[PDF](#)] [[PDF Plus](#)]
103. Tuan M. Nguyen, Pavel P. Popov, William A. Sirignano. Driving Mechanisms of Liquid-Propellant Rocket Longitudinal Combustion Instability . [[Citation](#)] [[PDF](#)] [[PDF Plus](#)]
104. James G. Coder, Thomas H. Pulliam, David Hue, Gaetan K. Kenway, Anthony J. Sclafani. Contributions to the 6th AIAA CFD Drag Prediction Workshop Using Structured Grid Methods . [[Citation](#)] [[PDF](#)] [[PDF Plus](#)]
105. Shervin Sammak, Arash G. Nouri, Michael J. Brazell, Dimitri J. Mavriplis, Peyman Givi. Discontinuous Galerkin-Monte Carlo Solver for Large Eddy Simulation of Compressible Turbulent Flows . [[Citation](#)] [[PDF](#)] [[PDF Plus](#)]
106. Rachit Prasad, Hyunsoon Kim, Seongim Choi. Adjoint based Finite Element Model Updating and Validation using Time Domain based FSI Analysis . [[Citation](#)] [[PDF](#)] [[PDF Plus](#)]
107. Antoine Joulain, Damien Desvigne, David Alfano, Thomas Leweke. 2017. Numerical Study of the Reliability of Wind-Tunnel Wall Corrections for Wingtip Flow. *Journal of Aircraft* 54:1, 354-358. [[Citation](#)] [[Full Text](#)] [[PDF](#)] [[PDF Plus](#)]
108. Christopher Lee, David Koo, David W. Zingg. 2017. Comparison of B-Spline Surface and Free-Form Deformation Geometry Control for Aerodynamic Optimization. *AIAA Journal* 55:1, 228-240. [[Abstract](#)] [[Full Text](#)] [[PDF](#)] [[PDF Plus](#)]
109. Vincent Poirier, Siva Nadarajah. 2016. Efficient Reduced-Radial Basis Function-Based Mesh Deformation Within an Adjoint-Based Aerodynamic Optimization Framework. *Journal of Aircraft* 53:6, 1905-1921. [[Abstract](#)] [[Full Text](#)] [[PDF](#)] [[PDF Plus](#)]
110. Ramy Rashad, David W. Zingg. 2016. Aerodynamic Shape Optimization for Natural Laminar Flow Using a Discrete-Adjoint Approach. *AIAA Journal* 54:11, 3321-3337. [[Abstract](#)] [[Full Text](#)] [[PDF](#)] [[PDF Plus](#)]
111. Jonas Verrière, Fabien Gand, Sébastien Deck. 2016. Zonal Detached-Eddy Simulations of a Dual-Stream Jet. *AIAA Journal* 54:10, 3176-3190. [[Abstract](#)] [[Full Text](#)] [[PDF](#)] [[PDF Plus](#)]
112. Xiao He, Xinqian Zheng. 2016. Mechanisms of Lean on the Performance of Transonic Centrifugal Compressor Impellers. *Journal of Propulsion and Power* 32:5, 1220-1229. [[Abstract](#)] [[Full Text](#)] [[PDF](#)] [[PDF Plus](#)]
113. Donald P. Rizzetta, Miguel R. Visbal. 2016. Simulation of Laminar-Flow Compatible High-Lift Wing Configuration with Flow Control. *Journal of Aircraft* 53:5, 1419-1430. [[Abstract](#)] [[Full Text](#)] [[PDF](#)] [[PDF Plus](#)]
114. David A. Brown, David W. Zingg. 2016. Performance of a Newton-Krylov-Schur Algorithm for Solving Steady Turbulent Flows. *AIAA Journal* 54:9, 2645-2658. [[Abstract](#)] [[Full Text](#)] [[PDF](#)] [[PDF Plus](#)]
115. Michael J. Brazell, Dimitri J. Mavriplis, Zhi Yang. 2016. Mesh-Resolved Airfoil Simulations Using Finite Volume and Discontinuous Galerkin Solvers. *AIAA Journal* 54:9, 2659-2670. [[Abstract](#)] [[Full Text](#)] [[PDF](#)] [[PDF Plus](#)]
116. Anand Amrit, Leifur T. Leifsson, Slawomir Koziel, Yonatan Afework Tesfahunegn. Efficient Multi-Objective Aerodynamic Optimization by Design Space Dimension Reduction and Co-Kriging . [[Citation](#)] [[PDF](#)] [[PDF Plus](#)]
117. Leifur T. Leifsson, Yonatan Afework Tesfahunegn, Slawomir Koziel. Aerodynamic Shape Optimization by Variable-fidelity Models and Gradient-Enhanced Manifold Mapping . [[Citation](#)] [[PDF](#)] [[PDF Plus](#)]
118. Rachit Prasad, Hyun Soon Kim, Dongkyun Im, Seongim Choi, Seulgi Yi. Analysis and Sensitivity Calculation using High Fidelity Spectral Formulation-Based FSI and Coupled Adjoint Method . [[Citation](#)] [[PDF](#)] [[PDF Plus](#)]
119. Carlos Junqueira-Junior, Sami Yamouni, Joao Luiz F. Azevedo, William Wolf. Influence of Different Subgrid Scale Models in LES of Supersonic Jet Flows . [[Citation](#)] [[PDF](#)] [[PDF Plus](#)]
120. Thomas D. Economou, Francisco Palacios, Sean R. Copeland, Trent W. Lukaczyk, Juan J. Alonso. 2016. SU2: An Open-Source Suite for Multiphysics Simulation and Design. *AIAA Journal* 54:3, 828-846. [[Abstract](#)] [[Full Text](#)] [[PDF](#)] [[PDF Plus](#)]
121. K. Hasanzadeh, E. Laurendeau, I. Paraschivoiu. 2016. Grid-Generation Algorithms for Complex Glaze-Ice Shapes Reynolds-Averaged Navier-Stokes Simulations. *AIAA Journal* 54:3, 847-860. [[Abstract](#)] [[Full Text](#)] [[PDF](#)] [[PDF Plus](#)]



122. R. G. Rajagopalan, Angela D. Lestari. 2016. RK-SIMPLER: Explicit Time-Accurate Algorithm for Incompressible Flows. *AIAA Journal* 54:2, 616-624. [[Abstract](#)] [[Full Text](#)] [[PDF](#)] [[PDF Plus](#)]
123. George N. Barakos, Antonio Jimenez-Garcia. Hover Predictions of the S-76 Rotor using HMB2 - Model to full Scale . [[Citation](#)] [[PDF](#)] [[PDF Plus](#)]
124. Antonio Jimenez-Garcia, George N. Barakos. CFD Simulations of the ERICA tiltrotor using HMB2 . [[Citation](#)] [[PDF](#)] [[PDF Plus](#)]
125. Slawomir Koziel, Yonatan Tesfahunegn, Anand Amrit, Leifur T. Leifsson. Rapid Multi-Objective Aerodynamic Design Using Co-Kriging and Space Mapping . [[Citation](#)] [[PDF](#)] [[PDF Plus](#)]
126. Jie Ren, Leifur T. Leifsson, Slawomir Koziel, Yonatan Tesfahunegn. Multi-Fidelity Aerodynamic Shape Optimization Using Manifold Mapping . [[Citation](#)] [[PDF](#)] [[PDF Plus](#)]
127. Lukas Wutschitz, Nikolaos Nikiforakis. A Cartesian Cut-Cell Approach for Modelling Air and Water Droplet Flow . [[Citation](#)] [[PDF](#)] [[PDF Plus](#)]
128. Rachit Prasad, Seulgi Yi, Seongim Choi, Dongkyun Im. Gradient Based Optimization using Spectral Formulation-Based FSI and Coupled Sensitivity Analysis . [[Citation](#)] [[PDF](#)] [[PDF Plus](#)]
129. David Koo, David W. Zingg. Progress in Aerodynamic Shape Optimization Based on the Reynolds-Averaged Navier-Stokes Equations . [[Citation](#)] [[PDF](#)] [[PDF Plus](#)]
130. Jae-Young Choi, Seongim Choi, Jangho Park, Dongkyun Im. Prediction of Dynamic Stability using Mapped Chebyshev Pseudospectral Method . [[Citation](#)] [[PDF](#)] [[PDF Plus](#)]
131. Jie Ren, Andrew S. Thelen, Anand Amrit, Xiaosong Du, Leifur T. Leifsson, Yonatan Tesfahunegn, Slawomir Koziel. Application of Multifidelity Optimization Techniques to Benchmark Aerodynamic Design Problems . [[Citation](#)] [[PDF](#)] [[PDF Plus](#)]
132. Jacques E. Peter, Jean-Antoine Desideri. Unstructured mesh adaptation for functional outputs. With application to two dimensionnal invscid flows . [[Citation](#)] [[PDF](#)] [[PDF Plus](#)]
133. Frédéric Moens, Julien Dandois. 2016. Optimization of Passive Flow Control Devices of a Slatless High-Lift Configuration. *Journal of Aircraft* 53:1, 189-201. [[Abstract](#)] [[Full Text](#)] [[PDF](#)] [[PDF Plus](#)]
134. Song Chen, Zhoujie Lyu, Gaetan K. W. Kenway, Joaquim R. R. A. Martins. 2016. Aerodynamic Shape Optimization of Common Research Model Wing-Body-Tail Configuration. *Journal of Aircraft* 53:1, 276-293. [[Abstract](#)] [[Full Text](#)] [[PDF](#)] [[PDF Plus](#)]
135. Aurélien Arntz, David Hue. 2016. Exergy-Based Performance Assessment of the NASA Common Research Model. *AIAA Journal* 54:1, 88-100. [[Abstract](#)] [[Full Text](#)] [[PDF](#)] [[PDF Plus](#)]
136. Donald P. Rizzetta, Miguel R. Visbal. 2016. Plasma-Based Control of Transition on a Wing with Leading-Edge Excrescence. *AIAA Journal* 54:1, 129-140. [[Abstract](#)] [[Full Text](#)] [[PDF](#)] [[PDF Plus](#)]
137. Gaetan K. W. Kenway, Joaquim R. R. A. Martins. 2016. Multipoint Aerodynamic Shape Optimization Investigations of the Common Research Model Wing. *AIAA Journal* 54:1, 113-128. [[Abstract](#)] [[Full Text](#)] [[PDF](#)] [[PDF Plus](#)] [[Supplementary Material](#)]
138. Dong Kyun Im, Seongim Choi, James E. McClure, Faith Skiles. 2015. Mapped Chebyshev Pseudospectral Method for Unsteady Flow Analysis. *AIAA Journal* 53:12, 3805-3820. [[Abstract](#)] [[Full Text](#)] [[PDF](#)] [[PDF Plus](#)]
139. Zhoujie Lyu, Joaquim R. R. A. Martins. 2015. Aerodynamic Shape Optimization of an Adaptive Morphing Trailing-Edge Wing. *Journal of Aircraft* 52:6, 1951-1970. [[Abstract](#)] [[Full Text](#)] [[PDF](#)] [[PDF Plus](#)]
140. Heyong Xu, Shilong Xing, Zhengyin Ye. 2015. Numerical Study of an Airfoil/Rotating-Slotted-Cylinder Based Flutter Exciter. *Journal of Aircraft* 52:6, 2100-2105. [[Citation](#)] [[Full Text](#)] [[PDF](#)] [[PDF Plus](#)]
141. Benjamin Walther, Siva Nadarajah. 2015. Adjoint-Based Constrained Aerodynamic Shape Optimization for Multistage Turbomachines. *Journal of Propulsion and Power* 31:5, 1298-1319. [[Abstract](#)] [[Full Text](#)] [[PDF](#)] [[PDF Plus](#)]
142. Andreas Hövelmann, Christian Breitsamter. 2015. Leading-Edge Geometry Effects on the Vortex Formation of a Diamond-Wing Configuration. *Journal of Aircraft* 52:5, 1596-1610. [[Abstract](#)] [[Full Text](#)] [[PDF](#)] [[PDF Plus](#)]
143. Heinrich Lüdeke, Jean Daniel Mulot, Klaus Hannemann. 2015. Launch Vehicle Base Flow Analysis Using Improved Delayed Detached-Eddy Simulation. *AIAA Journal* 53:9, 2454-2471. [[Abstract](#)] [[Full Text](#)] [[PDF](#)] [[PDF Plus](#)]
144. Thomas D. Economou, Francisco Palacios, Juan J. Alonso. 2015. Unsteady Continuous Adjoint Approach for Aerodynamic Design on Dynamic Meshes. *AIAA Journal* 53:9, 2437-2453. [[Abstract](#)] [[Full Text](#)] [[PDF](#)] [[PDF Plus](#)]
145. David Hue, Olivier Vermeersch, Didier Bailly, Vincent Brunet, Maxime Forte. 2015. Experimental and Numerical Methods for Transition and Drag Predictions of Laminar Airfoils. *AIAA Journal* 53:9, 2694-2712. [[Abstract](#)] [[Full Text](#)] [[PDF](#)] [[PDF Plus](#)]
146. G. Delattre, F. Falissard. 2015. Influence of Torque Ratio on Counter-Rotating Open-Rotor Interaction Noise. *AIAA Journal* 53:9, 2726-2738. [[Abstract](#)] [[Full Text](#)] [[PDF](#)] [[PDF Plus](#)]

147. Stefan Langer, Axel Schwöppe, Norbert Kroll. 2015. Investigation and Comparison of Implicit Smoothers Applied in Agglomeration Multigrid. *AIAA Journal* 53:8, 2080-2096. [[Abstract](#)] [[Full Text](#)] [[PDF](#)] [[PDF Plus](#)]
148. Zhichao Zhang, P. C. Chen, Shuchi Yang, Zhicun Wang, Qiqi Wang. 2015. Unsteady Aerostructure Coupled Adjoint Method for Flutter Suppression. *AIAA Journal* 53:8, 2121-2129. [[Abstract](#)] [[Full Text](#)] [[PDF](#)] [[PDF Plus](#)]
149. Antoine Despeyroux, Jean-Pierre Hickey, Robert Desaulnier, Ryan Luciano, Michael Piotrowski, Nicolas Hamel. 2015. Numerical Analysis of Static and Dynamic Performances of Grid Fin Controlled Missiles. *Journal of Spacecraft and Rockets* 52:4, 1236-1252. [[Abstract](#)] [[Full Text](#)] [[PDF](#)] [[PDF Plus](#)]
150. Daniel Destarac. 2015. Three-Component Breakdown of Spurious Drag in Computational Fluid Dynamics. *Journal of Aircraft* 52:4, 1336-1344. [[Abstract](#)] [[Full Text](#)] [[PDF](#)] [[PDF Plus](#)]
151. Thomas Jann, Sven Geisbauer, Niko Bier, Wolf Krüger, Hauke Schmidt. Multi-Fidelity Simulation of Cargo Airdrop: From the Payload Bay to the Ground . [[Citation](#)] [[PDF](#)] [[PDF Plus](#)]
152. Antony Jameson. Application of Dual Time Stepping to Fully Implicit Runge Kutta Schemes for Unsteady Flow Calculations . [[Citation](#)] [[PDF](#)] [[PDF Plus](#)]
153. Andrew C. Kirby, Dimitri J. Mavriplis, Andrew M. Wissink. An Adaptive Explicit 3D Discontinuous Galerkin Solver for Unsteady Problems . [[Citation](#)] [[PDF](#)] [[PDF Plus](#)]
154. Ramy Rashad, David W. Zingg. Aerodynamic Shape Optimization for Natural Laminar Flow Using a Discrete-Adjoint Approach . [[Citation](#)] [[PDF](#)] [[PDF Plus](#)]
155. Firat Kiyici, Selin Aradag. Design and Optimization of a Supersonic Business Jet . [[Citation](#)] [[PDF](#)] [[PDF Plus](#)]
156. Carlos Junqueira-Junior, Sami Yamouni, Joao Luiz F. Azevedo, William Wolf. Large Eddy Simulations of Supersonic Jet Flows for Aeroacoustic Applications . [[Citation](#)] [[PDF](#)] [[PDF Plus](#)]
157. David E. Manosalvas, Thomas D. Economon, Francisco Palacios, Antony Jameson. Techniques for the Design of Active Flow Control Systems in Heavy Vehicles . [[Citation](#)] [[PDF](#)] [[PDF Plus](#)]
158. Adèle Poubeau, Roberto Paoli, Antoine Dauplain, Florent Duchaine, Gaofeng Wang. 2015. Large-Eddy Simulations of a Single-Species Solid Rocket Booster Jet. *AIAA Journal* 53:6, 1477-1491. [[Abstract](#)] [[Full Text](#)] [[PDF](#)] [[PDF Plus](#)]
159. Zhoujie Lyu, Gaetan K. W. Kenway, Joaquim R. R. A. Martins. 2015. Aerodynamic Shape Optimization Investigations of the Common Research Model Wing Benchmark. *AIAA Journal* 53:4, 968-985. [[Abstract](#)] [[Full Text](#)] [[PDF](#)] [[PDF Plus](#)] [[Supplementary Material](#)]
160. Pascal Molton, David Hue, Reynald Bur. 2015. Drag Induced by Flat-Plate Imperfections in Compressible Turbulent Flow Regimes. *Journal of Aircraft* 52:2, 667-679. [[Abstract](#)] [[Full Text](#)] [[PDF](#)] [[PDF Plus](#)]
161. Michael Meheut, Daniel Destarac, Saloua Ben Khelil, Gerald Carrier, Antoine Dumont, Jacques Peter. Gradient-Based Single and Multi-points Aerodynamic Optimizations with the elsA Software . [[Citation](#)] [[PDF](#)] [[PDF Plus](#)]
162. Gaetan K. Kenway, David A. Burdette, Joaquim R. R. A. Martins. Multipoint Aerodynamic Shape Optimization Investigations of the Common Research Model Wing . [[Citation](#)] [[PDF](#)] [[PDF Plus](#)]
163. Kazem Hasanzadeh Lashkajani, Eric Laurendeau, Ion Paraschivoiu. Adaptive curvature control grid generation algorithms for complex glaze ice shapes RANS simulations . [[Citation](#)] [[PDF](#)] [[PDF Plus](#)]
164. Pierre-Olivier Tardif, Sivakumaran Nadarajah. Dynamic Mesh Deformation with Radial Basis Functions for the Non-Linear Frequency Domain Method . [[Citation](#)] [[PDF](#)] [[PDF Plus](#)]
165. Song Chen, Zhoujie Lyu, Gaetan K. Kenway, Joaquim R. R. A. Martins. Aerodynamic Shape Optimization of the Common Research Model Wing-Body-Tail Configuration . [[Citation](#)] [[PDF](#)] [[PDF Plus](#)]
166. David A. Brown, Howard Buckley, Michal Osusky, David W. Zingg. Performance of a Newton-Krylov-Schur Algorithm for the Numerical Solution of the Steady Reynolds-Averaged Navier-Stokes Equations (Invited) . [[Citation](#)] [[PDF](#)] [[PDF Plus](#)]
167. Jonathan Y. Kemal, Roger L. Davis, John D. Owens. Multidisciplinary Simulation Acceleration using Multiple Shared-Memory Graphical Processing Units . [[Citation](#)] [[PDF](#)] [[PDF Plus](#)]
168. Mohamed Bouriga, François Morency, Julien Weiss. Numerical Investigation of Wall Mounting Effects in Semi-Span Wind-Tunnel Tests . [[Citation](#)] [[PDF](#)] [[PDF Plus](#)]
169. Wei Liao, Mujeeb R. Malik, Elizabeth M. Lee-Rausch, Fei Li, Eric J. Nielsen, Pieter G. Buning, Meelan Choudhari, Chau-Lyan Chang. 2015. Boundary-Layer Stability Analysis of the Mean Flows Obtained Using Unstructured Grids. *Journal of Aircraft* 52:1, 49-63. [[Abstract](#)] [[Full Text](#)] [[PDF](#)] [[PDF Plus](#)]
170. C. Wales, D. Jones, A. Gaitonde. 2015. Prescribed Velocity Method for Simulation of Aerofoil Gust Responses. *Journal of Aircraft* 52:1, 64-76. [[Abstract](#)] [[Full Text](#)] [[PDF](#)] [[PDF Plus](#)]

171. Julien Dandois. 2014. Improvement of Corner Flow Prediction Using the Quadratic Constitutive Relation. *AIAA Journal* **52**:12, 2795-2806. [[Abstract](#)] [[Full Text](#)] [[PDF](#)] [[PDF Plus](#)]
172. Jerome de Laborderie, Stephane Moreau. 2014. Evaluation of a Cascade-Based Acoustic Model for Fan Tonal Noise Prediction. *AIAA Journal* **52**:12, 2877-2890. [[Abstract](#)] [[Full Text](#)] [[PDF](#)] [[PDF Plus](#)]
173. Jerome de Laborderie, Laurent Soulat, Stephane Moreau. 2014. Prediction of Noise Sources in Axial Compressor from URANS Simulation. *Journal of Propulsion and Power* **30**:5, 1257-1271. [[Abstract](#)] [[Full Text](#)] [[PDF](#)] [[PDF Plus](#)]
174. Huang Huang, Kivanc Ekici. 2014. Stabilization of High-Dimensional Harmonic Balance Solvers Using Time Spectral Viscosity. *AIAA Journal* **52**:8, 1784-1794. [[Abstract](#)] [[Full Text](#)] [[PDF](#)] [[PDF Plus](#)]
175. Olaf Brodersen, Simone Crippa, Bernhard Eisfeld, Stefan Keye, Sven Geisbauer. 2014. DLR Results from the Fourth AIAA Computational Fluid Dynamics Drag Prediction Workshop. *Journal of Aircraft* **51**:4, 1135-1148. [[Abstract](#)] [[Full Text](#)] [[PDF](#)] [[PDF Plus](#)]
176. David Hue. 2014. Fifth Drag Prediction Workshop: Computational Fluid Dynamics Studies Carried Out at ONERA. *Journal of Aircraft* **51**:4, 1295-1310. [[Abstract](#)] [[Full Text](#)] [[PDF](#)] [[PDF Plus](#)]
177. David Hue. 2014. Fifth Drag Prediction Workshop: ONERA Investigations with Experimental Wing Twist and Laminarity. *Journal of Aircraft* **51**:4, 1311-1322. [[Abstract](#)] [[Full Text](#)] [[PDF](#)] [[PDF Plus](#)]
178. Stefan Keye, Olaf Brodersen, Melissa B. Rivers. 2014. Investigation of Aeroelastic Effects on the NASA Common Research Model. *Journal of Aircraft* **51**:4, 1323-1330. [[Abstract](#)] [[Full Text](#)] [[PDF](#)] [[PDF Plus](#)]
179. Vamshi Togiti, Bernhard Eisfeld, Olaf Brodersen. 2014. Turbulence Model Study for the Flow Around the NASA Common Research Model. *Journal of Aircraft* **51**:4, 1331-1343. [[Abstract](#)] [[Full Text](#)] [[PDF](#)] [[PDF Plus](#)]
180. Zhoujie Lyu, Joaquim R. R. A. Martins. Strategies for Solving High-Fidelity Aerodynamic Shape Optimization Problems . [[Citation](#)] [[PDF](#)] [[PDF Plus](#)]
181. David R. Gonzalez, Datta V. Gaitonde, Mark J. Lewis. Exploratory Investigation of Asymmetric Control of a Supersonic Round Jet via Plasma Actuation . [[Citation](#)] [[PDF](#)] [[PDF Plus](#)]
182. Kui Ou, Antony Jameson, John C. Vassberg. Airfoils Supporting Non-unique Transonic Solutions for Unsteady Viscous Flows . [[Citation](#)] [[PDF](#)] [[PDF Plus](#)]
183. Kui Ou, Antony Jameson, John C. Vassberg. Studies of Wings Supporting Non-unique Solutions in Transonic Flows . [[Citation](#)] [[PDF](#)] [[PDF Plus](#)]
184. Braulio G. Pimenta, Roberto F. Bobenrieth Miserda. Direct Noise Computation of Linear and Nonlinear Rotor-Stator Interaction Modes in Transonic Cascades . [[Citation](#)] [[PDF](#)] [[PDF Plus](#)]
185. Zhoujie Lyu, Joaquim R. R. A. Martins. Aerodynamic Shape Optimization of an Adaptive Morphing Trailing Edge Wing . [[Citation](#)] [[PDF](#)] [[PDF Plus](#)]
186. Antoine Despeyroux, Robert Desaulnier, Ryan Luciano, Michael Piotrowski, Jean-Pierre Hickey, Xiaohua Wu, Nicolas Hamel, François Lesage. Numerical analysis of static and dynamic performances of grid fin controlled missiles . [[Citation](#)] [[PDF](#)] [[PDF Plus](#)]
187. Aaron Katz, Andrew M. Wissink. 2014. Efficient Solution Methods for Strand Grid Applications. *AIAA Journal* **52**:2, 267-280. [[Abstract](#)] [[Full Text](#)] [[PDF](#)] [[PDF Plus](#)]
188. Donald P. Rizzetta, Miguel R. Visbal. 2014. Numerical Simulation of Excrescence Generated Transition. *AIAA Journal* **52**:2, 385-397. [[Abstract](#)] [[Full Text](#)] [[PDF](#)] [[PDF Plus](#)]
189. Michal Osusky, David W. Zingg. Steady three-dimensional turbulent flow computations with a parallel Newton-Krylov-Schur algorithm . [[Citation](#)] [[PDF](#)] [[PDF Plus](#)]
190. Zhoujie Lyu, Gaetan K. Kenway, Joaquim R. R. A. Martins. RANS-based Aerodynamic Shape Optimization Investigations of the Common Research Model Wing . [[Citation](#)] [[PDF](#)] [[PDF Plus](#)]
191. Pranay Seshadri, Paul Constantine, Gianluca Iaccarino. Aggressive Design Under Uncertainty . [[Citation](#)] [[PDF](#)] [[PDF Plus](#)]
192. Frédéric Sicot, Adrien Gomar, Guillaume Dufour, Alain Dugeai. 2014. Time-Domain Harmonic Balance Method for Turbomachinery Aeroelasticity. *AIAA Journal* **52**:1, 62-71. [[Abstract](#)] [[Full Text](#)] [[PDF](#)] [[PDF Plus](#)]
193. Michal Osusky, David W. Zingg. 2013. Parallel Newton-Krylov-Schur Flow Solver for the Navier-Stokes Equations. *AIAA Journal* **51**:12, 2833-2851. [[Abstract](#)] [[Full Text](#)] [[PDF](#)] [[PDF Plus](#)]
194. Reik Thormann, Markus Widhalm. 2013. Linear-Frequency-Domain Predictions of Dynamic-Response Data for Viscous Transonic Flows. *AIAA Journal* **51**:11, 2540-2557. [[Abstract](#)] [[Full Text](#)] [[PDF](#)] [[PDF Plus](#)]

195. G. Aubard, X. Gloerfelt, J.-C. Robinet. 2013. Large-Eddy Simulation of Broadband Unsteadiness in a Shock/Boundary-Layer Interaction. *AIAA Journal* **51**:10, 2395-2409. [[Abstract](#)] [[Full Text](#)] [[PDF](#)] [[PDF Plus](#)]
196. Nicholas J. Bisek, Donald P. Rizzetta, Jonathan Poggie. 2013. Plasma Control of a Turbulent Shock Boundary-Layer Interaction. *AIAA Journal* **51**:8, 1789-1804. [[Abstract](#)] [[Full Text](#)] [[PDF](#)] [[PDF Plus](#)]
197. Weimin Sang, Yu Shi. 2013. Comparison of Octree and Omni-Tree Cartesian Grid for Civil-Plane High-Lift Model Simulations. *Journal of Aircraft* **50**:4, 1099-1105. [[Abstract](#)] [[Full Text](#)] [[PDF](#)] [[PDF Plus](#)]
198. Andre C. Marta, Sriram Shankaran, Qiqi Wang, Prem Venugopal. 2013. Interpretation of Adjoint Solutions for Turbomachinery Flows. *AIAA Journal* **51**:7, 1733-1744. [[Abstract](#)] [[Full Text](#)] [[PDF](#)] [[PDF Plus](#)]
199. Michal Osusky, Pieter D. Boom, David W. Zingg. Results from the Fifth AIAA Drag Prediction Workshop obtained with a parallel Newton-Krylov-Schur flow solver discretized using summation-by-parts operators . [[Citation](#)] [[PDF](#)] [[PDF Plus](#)]
200. Ramy Rashad, David W. Zingg. Toward High-Fidelity Aerodynamic Shape Optimization for Natural Laminar Flow . [[Citation](#)] [[PDF](#)] [[PDF Plus](#)]
201. Ya Liu, Juntao Xiong, Feng Liu, Shijun Luo. Non-unique Numerical Solutions and Their Stability of the Euler Equations for Transonic Flow over Airfoils . [[Citation](#)] [[PDF](#)] [[PDF Plus](#)]
202. C. Marongiu, Frank Tarfeld, Harry Adirim, Norbert A. Pilz. Dynamic Derivative Computation of a Sub-orbital Vehicle . [[Citation](#)] [[PDF](#)] [[PDF Plus](#)]
203. Eirene Rebecca Busch, Manuel Kessler, Ewald Kraemer. Aeroacoustics of a High-Fidelity CFD Calculation of a Counter-Rotating Open Rotor in Take-Off Conditions . [[Citation](#)] [[PDF](#)] [[PDF Plus](#)]
204. Roberto F. Bobenrieth Miserda, Braulio G. Pimenta, Rafael L. Bites, Ana Luisa Maldonado. Validation of a Moving-Body High-Order Immersed Boundary Method for Direct Tonal Noise Predictions of Rotor-Stator Interactions . [[Citation](#)] [[PDF](#)] [[PDF Plus](#)]
205. Kivanc Ekici, Kenneth C. Hall, Huang Huang, Jeffrey P. Thomas. 2013. Stabilization of Explicit Flow Solvers Using a Proper-Orthogonal-Decomposition Technique. *AIAA Journal* **51**:5, 1095-1104. [[Abstract](#)] [[Full Text](#)] [[PDF](#)] [[PDF Plus](#)]
206. Thomas Jann, Sven Geisbauer. Approximated Steady Aerodynamic Characteristics for two Cuboids and a Hemispherical Shell used in Airdrop Simulation . [[Citation](#)] [[PDF](#)] [[PDF Plus](#)]
207. Lionel Castillon, Guillaume Legras. 2013. Overset Grid Method for Simulation of Compressors with Nonaxisymmetric Casing Treatment. *Journal of Propulsion and Power* **29**:2, 460-465. [[Abstract](#)] [[Full Text](#)] [[PDF](#)] [[PDF Plus](#)]
208. Ali Mosahebi Mohamadi, Sivakumaran Nadarajah. Algorithmic Advanced for the Adaptive Non-Linear Frequency Domain Method . [[Citation](#)] [[PDF](#)] [[PDF Plus](#)]
209. Alireza Jalali, Carl Ollivier Gooch. Accuracy Assessment of Finite Volume Discretizations of Convective Fluxes on Unstructured Meshes . [[Citation](#)] [[PDF](#)] [[PDF Plus](#)]
210. Maren Matter, Eirene Busch, Thorsten Lutz, Manuel Kessler, Ewald Kraemer. Numerical investigation of a model propeller operating under off-design conditions . [[Citation](#)] [[PDF](#)] [[PDF Plus](#)]
211. Vlad Ciobaca, Timo Kühn, Ralf Rudnik, Matthias Bauer, Burkhard Gölling, Wiebke Breitenstein. 2013. Active Flow-Separation Control on a High-Lift Wing-Body Configuration. *Journal of Aircraft* **50**:1, 56-72. [[Abstract](#)] [[Full Text](#)] [[PDF](#)] [[PDF Plus](#)]
212. Juntao Xiong, Feng Liu, Dimitri Papamoschou. 2012. Aerodynamic Performance of Fan-Flow Deflectors for Jet-Noise Reduction. *Journal of Propulsion and Power* **28**:4, 728-738. [[Citation](#)] [[PDF](#)] [[PDF Plus](#)]
213. Markus O. Burak, Lars-Erik Eriksson, David Munday, Ephraim Gutmark, Erik Prisell. 2012. Experimental and Numerical Investigation of a Supersonic Convergent-Divergent Nozzle. *AIAA Journal* **50**:7, 1462-1475. [[Citation](#)] [[PDF](#)] [[PDF Plus](#)]
214. A. Dauplain, L. Y. M. Gicquel, S. Moreau. 2012. Large Eddy Simulation of Supersonic Impinging Jets. *AIAA Journal* **50**:7, 1560-1574. [[Citation](#)] [[PDF](#)] [[PDF Plus](#)]
215. Simone Crippa, Normann Krimmelbein. Transitional Flow Computations of the NASA Trapezoidal Wing with the DLR TAU Code . [[Citation](#)] [[PDF](#)] [[PDF Plus](#)]
216. Benjamin Kutz, Ulrich Kowarsch, Manuel Kessler, Ewald Kraemer. Numerical Investigation of Helicopter Rotors in Ground Effect . [[Citation](#)] [[PDF](#)] [[PDF Plus](#)]
217. Z. Zhang, S. Yang, P. C. Chen. 2012. Linearized Euler Solver for Rapid Frequency-Domain Aeroelastic Analysis. *Journal of Aircraft* **49**:3, 922-932. [[Citation](#)] [[PDF](#)] [[PDF Plus](#)]
218. Justin Jaworski, Raymond Gordnier. Thrust Augmentation of Flapping Airfoils in Low Reynolds Number Flow Using a Flexible Membrane . [[Citation](#)] [[PDF](#)] [[PDF Plus](#)]
219. Nicolas Gourdain, Laurent Y. M. Gicquel, Elena Collado. 2012. RANS and LES for the Heat Transfer Prediction in Turbine Guide Vane. *Journal of Propulsion and Power* **28**:2, 423-433. [[Citation](#)] [[PDF](#)] [[PDF Plus](#)]



220. He-yong Xu, Zheng-yin Ye, Ai-ming Shi. 2012. Numerical Study of Propeller Slipstream Based on Unstructured Dynamic Overset Grids. *Journal of Aircraft* **49**:2, 384-389. [Citation] [PDF] [PDF Plus]
221. Kaveh Mohamed, Siva Nadarajah, Marius Paraschivoiu. 2012. Eddy-Preserving Limiter for Unsteady Subsonic Flows. *AIAA Journal* **50**:2, 429-446. [Citation] [PDF] [PDF Plus]
222. Michal Osusky, David Zingg. A parallel Newton-Krylov-Schur flow solver for the Reynolds-Averaged Navier-Stokes equations. [Citation] [PDF] [PDF Plus]
223. Peyman Khayatzaheh, Sivakumaran Nadarajah. Aerodynamic Shape Optimization of Natural Laminar Flow (NLF) Airfoils. [Citation] [PDF] [PDF Plus]
224. Benjamin Walther, Sivakumaran Nadarajah. Constrained Adjoint-Based Aerodynamic Shape Optimization in a Multistage Turbomachinery Environment. [Citation] [PDF] [PDF Plus]
225. Everett H. Phillips, Yao Zhang, Roger L. Davis, John D. Owens. 2011. Acceleration of 2-D Compressible Flow Solvers with Graphics Processing Unit Clusters. *Journal of Aerospace Computing, Information, and Communication* **8**:8, 237-249. [Citation] [PDF] [PDF Plus]
226. Roberto F. Bobenrieth Miserda, Ana Maldonado, Braulio Gutierrez. A Moving-Body High-Order Immersed Boundary Method for Computational Aeroacoustics. [Citation] [PDF] [PDF Plus]
227. Simone Crippa. 2011. Improvement of Unstructured Computational Fluid Dynamics Simulations Through Novel Mesh Generation Methodologies. *Journal of Aircraft* **48**:3, 1036-1044. [Citation] [PDF] [PDF Plus]
228. Alejandro Lorenzo, Eusebio Valero, Valentín De-Pablo. DES/DDES Post-Stall Study with Iced Airfoil. [Citation] [PDF] [PDF Plus]
229. Justin Jaworski, Raymond Gordnier. High-Order Simulations of Low Reynolds Number Membrane Airfoils under Prescribed Motion. [Citation] [PDF] [PDF Plus]
230. Marcus Vinicius Ramalho, Joao Henrique Azevedo, Joao Luiz Azevedo. Further Investigation into the Origin of the Carbuncle Phenomenon in Aerodynamic Simulations. [Citation] [PDF] [PDF Plus]
231. Peyman Khayatzaheh, Siva Nadarajah. Aerodynamic Shape Optimization via Discrete Viscous Adjoint Equations for the k- $\omega$ SST Turbulence and  $\gamma$ -Re $\theta$  Transition Models. [Citation] [PDF] [PDF Plus]
232. Cetin Kiris, Jeffrey Housman, Marshall Gusman, Daniel Schauerhamer, Karen Deere, Alaa Elmiligui, Khaled Abdol-Hamid, Edward Parlette, Mark Andrews, John Blevins. Best Practices for Aero-Database CFD Simulations of Ares V Ascent. [Citation] [PDF] [PDF Plus]
233. Hugo Almeida, Joao Luiz Azevedo. Investigation of Viscous Effects on the Aeroelastic Stability of Transonic Airfoils. [Citation] [PDF] [PDF Plus]
234. F. Blanc, F.-X. Roux, J.-C. Jouhaud. 2010. Harmonic-Balance-Based Code-Coupling Algorithm for Aeroelastic Systems Subjected to Forced Excitation. *AIAA Journal* **48**:11, 2472-2481. [Citation] [PDF] [PDF Plus]
235. Aaron Katz, Antony Jameson. 2010. Meshless Scheme Based on Alignment Constraints. *AIAA Journal* **48**:11, 2501-2511. [Citation] [PDF] [PDF Plus]
236. C. Marongiu, R. Tognaccini. 2010. Far-Field Analysis of the Aerodynamic Force by Lamb Vector Integrals. *AIAA Journal* **48**:11, 2543-2555. [Citation] [PDF] [PDF Plus]
237. Thomas Schmitt, Laurent Selle, Anthony Ruiz, Bénédicte Cuenot. 2010. Large-Eddy Simulation of Supercritical-Pressure Round Jets. *AIAA Journal* **48**:9, 2133-2144. [Citation] [PDF] [PDF Plus]
238. Juntao Xiong, Feng Liu, Dimitri Papamoschou. Computation of the Flow of a Dual-Stream Jet with External Solid and Perforated Wedge Deflectors for Noise Reduction. [Citation] [PDF] [PDF Plus]
239. Alberto Nogueira, Renato Cantao, Claudio Silva, Enda Bigarella. Development of a Commercial CFD Tool Based on a Discontinuous Galerkin Formulation. [Citation] [PDF] [PDF Plus]
240. Roberto Bobenrieth Miserda, Ana Luisa Maldonado, Braulio Pimenta, Rudner Queiroz. Simulation of the Cascade-Gust Interaction Problem Using a High-Order Immersed Boundary Method. [Citation] [PDF] [PDF Plus]
241. Jason E. Hicken, David W. Zingg. 2010. Aerodynamic Optimization Algorithm with Integrated Geometry Parameterization and Mesh Movement. *AIAA Journal* **48**:2, 400-413. [Citation] [PDF] [PDF Plus]
242. Michal Osusky, Jason Hicken, David Zingg. A Parallel Newton-Krylov-Schur Flow Solver for the Navier-Stokes Equations Using the SBP-SAT Approach. [Citation] [PDF] [PDF Plus]
243. Edmond Kwan-yu Chiu, Antony Jameson. An Edge-Averaged Semi-Meshless Framework for Numerical Solution of Conservation Laws. [Citation] [PDF] [PDF Plus]

244. Marcus Ramalho, Joao Luiz Azevedo. A Possible Mechanism for the Appearance of the Carbuncle Phenomenon in Aerodynamic Simulations . [\[Citation\]](#) [\[PDF\]](#) [\[PDF Plus\]](#)
245. Tijmen Ton, Arjen Koop, Harry Hoeijmakers, Hein de Vries. Investigation of Vorticity Confinement in Compressible Flow . [\[Citation\]](#) [\[PDF\]](#) [\[PDF Plus\]](#)
246. Roberto Bobenrieth Miserda, Rudner Lauterjung Queiroz, Ana Luisa Maldonado, Isadora Ribeiro, Kerson Godoy, Oswaldo Neto. Direct Computation of Noise Generated by Complex Geometries Using a High-Order Immersed Boundary Method . [\[Citation\]](#) [\[PDF\]](#) [\[PDF Plus\]](#)
247. Shyam Sundar Dhanabalan, Khoon Seng Yeo. Riemann Solvers on Extended Domains for Higher Order Schemes . [\[Citation\]](#) [\[PDF\]](#) [\[PDF Plus\]](#)
248. Everett Phillips, Yao Zhang, Roger Davis, John Owens. Rapid Aerodynamic Performance Prediction on a Cluster of Graphics Processing Units . [\[Citation\]](#) [\[PDF\]](#) [\[PDF Plus\]](#)
249. Aaron Katz, Antony Jameson. A Comparison of Various Meshless Schemes Within a Unified Algorithm . [\[Citation\]](#) [\[PDF\]](#) [\[PDF Plus\]](#)
250. Jason E. Hicken, David W. Zingg. 2008. Parallel Newton-Krylov Solver for the Euler equations Discretized Using Simultaneous Approximation Terms. *AIAA Journal* **46**:11, 2773-2786. [\[Citation\]](#) [\[PDF\]](#) [\[PDF Plus\]](#)
251. Nawee Butsumtorn, Antony Jameson. Time Spectral Method for Rotorcraft Flow with Vorticity Confinement . [\[Citation\]](#) [\[PDF\]](#) [\[PDF Plus\]](#)
252. Antonio Baeza, Carlos Castro, Francisco Palacios, Enrique Zuazua. 2D Euler Shape Design on Non-Regular Flows Using Adjoint Rankine-Hugoniot Relations . [\[Citation\]](#) [\[PDF\]](#) [\[PDF Plus\]](#)
253. Antonio Baeza, Carlos Castro, Francisco Palacios, Enrique Zuazua. 2D Navier-Stokes Shape Design Using a Level Set Method . [\[Citation\]](#) [\[PDF\]](#) [\[PDF Plus\]](#)
254. Nawee Butsumtorn, Antony Jameson. Time Spectral Method for Rotorcraft Flow . [\[Citation\]](#) [\[PDF\]](#) [\[PDF Plus\]](#)
255. Lisa Carolina, Her Mann Tsai, Feng Liu. An Embedded Cartesian Grid Euler Solver with Radial Basis Function for Boundary Condition Implementation . [\[Citation\]](#) [\[PDF\]](#) [\[PDF Plus\]](#)
256. Aaron Katz, Antony Jameson. Edge-Based Meshless Methods for Compressible Flow Simulations . [\[Citation\]](#) [\[PDF\]](#) [\[PDF Plus\]](#)
257. Alexandre Noll Marques, João Luiz F. Azevedo. 2007. Application of CFD-Based Unsteady Forces for Efficient Aeroelastic Stability Analyses. *Journal of Aircraft* **44**:5, 1499-1512. [\[Citation\]](#) [\[PDF\]](#) [\[PDF Plus\]](#)
258. F. M. Najjar, J. P. Ferry, A. Haselbacher, S. Balachandar. 2006. Simulations of Solid-Propellant Rockets: Effects of Aluminum Droplet Size Distribution. *Journal of Spacecraft and Rockets* **43**:6, 1258-1270. [\[Citation\]](#) [\[PDF\]](#) [\[PDF Plus\]](#)
259. Robert Fiedler, Bono Wasistho, Mark Brandyberry. Full 3-D Simulation of Turbulent Flow in the RSRM . [\[Citation\]](#) [\[PDF\]](#) [\[PDF Plus\]](#)
260. Alexandre Marques, Joao Azevedo. Application of CFD-Based Unsteady Forces for Efficient Aeroelastic Stability Analysis . [\[Citation\]](#) [\[PDF\]](#) [\[PDF Plus\]](#)
261. X. Q. Xing, M. Damodaran. 2005. Inverse Design of Transonic Airfoils Using Parallel Simultaneous Perturbation Stochastic Approximation. *Journal of Aircraft* **42**:2, 568-570. [\[Citation\]](#) [\[PDF\]](#) [\[PDF Plus\]](#)
262. X. Q. Xing, M. Damodaran. 2005. Application of Simultaneous Perturbation Stochastic Approximation Method for Aerodynamic Shape Design Optimization. *AIAA Journal* **43**:2, 284-294. [\[Citation\]](#) [\[PDF\]](#) [\[PDF Plus\]](#)
263. Enda Bigarella, Joao Azevedo. A Study of Convective Flux Computation Schemes for Aerodynamic Flows . [\[Citation\]](#) [\[PDF\]](#) [\[PDF Plus\]](#)
264. Enda Dimitri Bigarella, Edson Basso, Joao Luiz Azevedo. Centered and Upwind Multigrid Turbulent Flow Simulations with Applications to Launch Vehicles . [\[Citation\]](#) [\[PDF\]](#) [\[PDF Plus\]](#)
265. Vladimir Golubev, Reda Mankbadi. STMA Study of Airfoil Nonlinear Interaction with Unsteady Flow . [\[Citation\]](#) [\[PDF\]](#) [\[PDF Plus\]](#)
266. Vladimir Golubev, Axel Rohde. Application of Space-Time Mapping Analysis Method to Unsteady Nonlinear Gust-Airfoil Interaction Problem . [\[Citation\]](#) [\[PDF\]](#) [\[PDF Plus\]](#)
267. Chee Meng Tan, T. Ray, H. M. Tsai. A Comparative Study of Evolutionary Algorithm and Swarm Algorithm for Airfoil Shape Optimization Problems . [\[Citation\]](#) [\[PDF\]](#) [\[PDF Plus\]](#)
268. William Calhoon. HEAT RELEASE AND COMPRESSIBILITY EFFECTS ON PLANAR SHEAR LAYER DEVELOPMENT . [\[Citation\]](#) [\[PDF\]](#) [\[PDF Plus\]](#)

269. W. Calhoo, C. Kannepalli, J. Papp, S. Dash. Analysis of scalar fluctuations at high convective Mach numbers . [\[Citation\]](#) [\[PDF\]](#) [\[PDF Plus\]](#)
270. R. von Kaenel, N. Adams, L. Kleiser, J. Vos. An approximate deconvolution model for large-eddy simulation of compressible flows with finite-volume schemes . [\[Citation\]](#) [\[PDF\]](#) [\[PDF Plus\]](#)
271. M. Khalid, F. Zhang. The aerodynamic studies of aircraft wings with leading edge deformations due to accreted ice . [\[Citation\]](#) [\[PDF\]](#) [\[PDF Plus\]](#)
272. J. Papp, K. Ghia. Application of the RNG turbulence model to the simulation of axisymmetric supersonic separated base flows . [\[Citation\]](#) [\[PDF\]](#) [\[PDF Plus\]](#)
273. M. Kermani, E. Plett. Roe scheme in generalized coordinates. II - Application to inviscid and viscous flows . [\[Citation\]](#) [\[PDF\]](#) [\[PDF Plus\]](#)
274. Andreas Haselbacher, Jiri Blazek. 2000. Accurate and Efficient Discretization of Navier-Stokes Equations on Mixed Grids. *AIAA Journal* **38**:11, 2094-2102. [\[Citation\]](#) [\[PDF\]](#) [\[PDF Plus\]](#)
275. V. Ahuja, Y. Ozyoruk, L. Long. Computational simulations of fore and aft radiation from ducted fans . [\[Citation\]](#) [\[PDF\]](#) [\[PDF Plus\]](#)
276. Gerd Fritsch, Martin Hoeger, Cristoph Blaha, Dirk Bauer. 2000. Viscous Three-Dimensional Simulation of Transonic Compressor Stage on Parallel Hardware. *Journal of Propulsion and Power* **16**:3, 388-396. [\[Citation\]](#) [\[PDF\]](#) [\[PDF Plus\]](#)
277. Frederic Thivet, Valerie Saint-Martin, Olivier Leschiera. Assessment of turbulence models for transonic flows around supercritical airfoil computed with a zonal method . [\[Citation\]](#) [\[PDF\]](#) [\[PDF Plus\]](#)
278. David P. Lockard, Philip J. Morris. 1998. Wing-Tip Vortex Calculations Using a High-Accuracy Scheme. *Journal of Aircraft* **35**:5, 728-738. [\[Citation\]](#) [\[PDF\]](#) [\[PDF Plus\]](#)
279. C. Allen. On grid dependence of multi-bladed rotor solutions . [\[Citation\]](#) [\[PDF\]](#) [\[PDF Plus\]](#)
280. David P. Lockard, Philip J. Morris. 1998. Radiated Noise from Airfoils in Realistic Mean Flows. *AIAA Journal* **36**:6, 907-914. [\[Citation\]](#) [\[PDF\]](#) [\[PDF Plus\]](#)
281. John Papp, K. Ghia. Study of turbulent compressible mixing layers using two-equation turbulence models including an RNG k-epsilon model . [\[Citation\]](#) [\[PDF\]](#) [\[PDF Plus\]](#)
282. John Papp, K. Ghia. Implementation of an RNG k-epsilon turbulence model into version 3.0 of the NPARC 2-D Navier-Stokes flow solver . [\[Citation\]](#) [\[PDF\]](#) [\[PDF Plus\]](#)
283. M. Serpico, A. Ciucci, P. Bellomi, M. Fabrizi, D. Falconi, M. Amato, P. Bellomi, M. Fabrizi, D. Falconi, M. Amato, M. Serpico, A. Ciucci. Computational analysis for predicting aerodynamic performances of the VEGA Lightsat Launcher . [\[Citation\]](#) [\[PDF\]](#) [\[PDF Plus\]](#)
284. Gerd Fritsch, Martin Hoeger, Cristoph Blaha, Dirk Bauer. Viscous three-dimensional simulation of transonic compressor stage on parallel hardware . [\[Citation\]](#) [\[PDF\]](#) [\[PDF Plus\]](#)
285. E. Shalman, A. Yakhot, S. Shalman, O. Igra, Y. Yadlin, E. Shalman, A. Yakhot, S. Shalman, O. Igra, Y. Yadlin. An accurate computation of Navier-Stokes turbulent boundary layers by attenuating artificial dissipation . [\[Citation\]](#) [\[PDF\]](#) [\[PDF Plus\]](#)
286. P. Friedmann, D. Guillot, E. Presente, P. Friedmann, D. Guillot, E. Presente. Adaptive control of aeroelastic instabilities in transonic flow and its scaling . [\[Citation\]](#) [\[PDF\]](#) [\[PDF Plus\]](#)
287. V. Saint-Martin, F. Thivet, V. Saint-Martin, F. Thivet. Improvements of a zonal method for the computation of viscous separated flows . [\[Citation\]](#) [\[PDF\]](#) [\[PDF Plus\]](#)
288. Y. Kallinderis, H. McMorris. 1995. Magnitude of artificial dissipation for numerical simulations. *AIAA Journal* **33**:8, 1526-1529. [\[Citation\]](#) [\[PDF\]](#) [\[PDF Plus\]](#)
289. Oh Joon Kwon, Chunill Hah. 1995. Simulation of three-dimensional turbulent flows on unstructured meshes. *AIAA Journal* **33**:6, 1081-1089. [\[Citation\]](#) [\[PDF\]](#) [\[PDF Plus\]](#)
290. Gregory Spragle, Wayne Smith, Jonathan Weiss. Hanging node solution adaption on unstructured grids . [\[Citation\]](#) [\[PDF\]](#) [\[PDF Plus\]](#)
291. Y. Kallinderis, K. Nakajima. 1994. Finite element method for incompressible viscous flows with adaptive hybrid grids. *AIAA Journal* **32**:8, 1617-1625. [\[Citation\]](#) [\[PDF\]](#) [\[PDF Plus\]](#)
292. Oh Kwon, Chunill Hah. Solution of the 3-D Navier-Stokes equations with a two-equation turbulence model on unstructured meshes applied to turbomachinery . [\[Citation\]](#) [\[PDF\]](#) [\[PDF Plus\]](#)
293. H. Hefazi, V. Chin, L. T. Chen. 1994. Two-dimensional Euler zonal method using composite structured and unstructured meshes. *Journal of Aircraft* **31**:3, 651-658. [\[Citation\]](#) [\[PDF\]](#) [\[PDF Plus\]](#)

294. Timothy Nobel, Perry Wooden, Robert Arledge. Experimental thrust reverser design with computational analysis . [\[Citation\]](#) [\[PDF\]](#) [\[PDF Plus\]](#)
295. A. J. White, J. B. Young. 1993. Time-marching method for the prediction of two-dimensional, unsteady flows of condensing steam. *Journal of Propulsion and Power* **9**:4, 579-587. [\[Citation\]](#) [\[PDF\]](#) [\[PDF Plus\]](#)
296. OH KWON, CHUNILL HAH. Three-dimensional unstructured grid Euler method applied to turbine blades . [\[Citation\]](#) [\[PDF\]](#) [\[PDF Plus\]](#)
297. CHAO-HO SUNG, MICHAEL GRIFFIN, JEFF TSAI, THOMAS HUANG. Incompressible flow computation of forces and moments on bodies of revolution at incidence . [\[Citation\]](#) [\[PDF\]](#) [\[PDF Plus\]](#)
298. G. Volpe. 1993. Performance of compressible flow codes at low Mach numbers. *AIAA Journal* **31**:1, 49-56. [\[Citation\]](#) [\[PDF\]](#) [\[PDF Plus\]](#)
299. Kevin McGrattan. 1992. Comparison of transonic flow models. *AIAA Journal* **30**:9, 2340-2343. [\[Citation\]](#) [\[PDF\]](#) [\[PDF Plus\]](#)
300. F. Grasso, M. Marini, M. Passalacqua. 1992. Viscous high-speed flow computations by adaptive mesh embedding techniques. *AIAA Journal* **30**:7, 1780-1788. [\[Citation\]](#) [\[PDF\]](#) [\[PDF Plus\]](#)
301. Anutosh Moitra. 1992. Enthalpy damping for high Mach number Euler solutions. *AIAA Journal* **30**:2, 300-301. [\[Citation\]](#) [\[PDF\]](#) [\[PDF Plus\]](#)
302. T. CEBECI, A. KHATTAB, H. CHEN, L. CHEN. An approach to the design of wings - The role of mathematics, physics and economics . [\[Citation\]](#) [\[PDF\]](#) [\[PDF Plus\]](#)
303. Neal T. Frink. 1992. Upwind scheme for solving the Euler equations on unstructured tetrahedral meshes. *AIAA Journal* **30**:1, 70-77. [\[Citation\]](#) [\[PDF\]](#) [\[PDF Plus\]](#)
304. A. A. Hassan, L. N. Sankar. 1992. Separation control using moving surface effects - A numerical simulation. *Journal of Aircraft* **29**:1, 131-139. [\[Citation\]](#) [\[PDF\]](#) [\[PDF Plus\]](#)
305. Aparajit J. Mahajan, Earl H. Dowell, Donald B. Bliss. 1991. Role of artificial viscosity in Euler and Navier-Stokes solvers. *AIAA Journal* **29**:4, 555-559. [\[Citation\]](#) [\[PDF\]](#) [\[PDF Plus\]](#)
306. D. R. Reddy, G. J. Harloff. 1991. Three-dimensional viscous flow computations of high area ratio nozzles for hypersonic propulsion. *Journal of Propulsion and Power* **7**:1, 84-89. [\[Citation\]](#) [\[PDF\]](#) [\[PDF Plus\]](#)
307. P. Raj, J. M. Keen, S. W. Singer. 1990. Applications of an Euler aerodynamic method to free-vortex flow simulation. *Journal of Aircraft* **27**:11, 941-949. [\[Citation\]](#) [\[PDF\]](#) [\[PDF Plus\]](#)
308. Ridha Abid, Veer N. Vatsa, Dennis A. Johnson, Bruce W. Wedan. 1990. Prediction of separated transonic wing flows with nonequilibrium algebraic turbulence model. *AIAA Journal* **28**:8, 1426-1431. [\[Citation\]](#) [\[PDF\]](#) [\[PDF Plus\]](#)
309. L. CHEN, M. BUI. An interactive scheme for transonic wing/body flows based on Euler and inverse boundary-layer equations . [\[Citation\]](#) [\[PDF\]](#) [\[PDF Plus\]](#)
310. Rodrick V. Chima, Jeffrey W. Yokota. 1990. Numerical analysis of three-dimensional viscous internal flows. *AIAA Journal* **28**:5, 798-806. [\[Citation\]](#) [\[PDF\]](#) [\[PDF Plus\]](#)
311. Dimitri J. Mavriplis. 1990. Accurate multigrid solution of the Euler equations on unstructured and adaptive meshes. *AIAA Journal* **28**:2, 213-221. [\[Citation\]](#) [\[PDF\]](#) [\[PDF Plus\]](#)
312. FRANK CANNIZZARO, ALAA ELMILIGUI, N. MELSON, E. VON LAVANTE. A multiblock multigrid method for the solution of the three-dimensional Euler equations . [\[Citation\]](#) [\[PDF\]](#) [\[PDF Plus\]](#)
313. Y.-L. TSAI, K.-C. HSIEH. Comparative study of computational efficiency of two LU schemes for non-equilibrium reacting flows . [\[Citation\]](#) [\[PDF\]](#) [\[PDF Plus\]](#)
314. T. Q. Dang. 1989. Simulations of propeller/airframe interference effects using an Euler correction method. *Journal of Aircraft* **26**:11, 994-1001. [\[Citation\]](#) [\[PDF\]](#) [\[PDF Plus\]](#)
315. M. G. Macaraeg. 1989. Numerical models of two complex hypersonic flowfields. *Journal of Thermophysics and Heat Transfer* **3**:2, 97-104. [\[Citation\]](#) [\[PDF\]](#) [\[PDF Plus\]](#)
316. M. SICLARI. Three-dimensional hybrid finite volume solutions to the Euler equations for supersonic/hypersonic aircraft . [\[Citation\]](#) [\[PDF\]](#) [\[PDF Plus\]](#)
317. THOMAS PULLIAM. A computational challenge - Euler solution for ellipses . [\[Citation\]](#) [\[PDF\]](#) [\[PDF Plus\]](#)
318. GEORGE DULIKRACH. Artificial dissipation sensors for computational gasdynamics . [\[Citation\]](#) [\[PDF\]](#) [\[PDF Plus\]](#)
319. D. A. Caughey, R. K. Iyer. 1989. Diagonal implicit multigrid calculation of inlet flowfields. *AIAA Journal* **27**:1, 110-112. [\[Citation\]](#) [\[PDF\]](#) [\[PDF Plus\]](#)
320. J. M. Floryan. 1989. Goertler instability of wall jets. *AIAA Journal* **27**:1, 112-114. [\[Citation\]](#) [\[PDF\]](#) [\[PDF Plus\]](#)



321. Magdi H. Rizk, Donald R. Lovell, Timothy J. Baker. 1989. Euler procedure for three-dimensional transonic wall interference. *Journal of Aircraft* **26**:1, 48-55. [[Citation](#)] [[PDF](#)] [[PDF Plus](#)]
322. Magdi H. Rizk, Donald R. Lovell, Timothy J. Baker. 1988. Euler procedure for correcting two-dimensional transonic wind-tunnelwall interference. *AIAA Journal* **26**:12, 1457-1466. [[Citation](#)] [[PDF](#)] [[PDF Plus](#)]
323. Murali Damodaran, David A. Caughey. 1988. Finite-volume calculation of inviscid transonic airfoil-vortex interaction. *AIAA Journal* **26**:11, 1346-1353. [[Citation](#)] [[PDF](#)] [[PDF Plus](#)]
324. P. Raj, J. S. Sikora, J. M. Keen. 1988. Free-vortex flow simulation using a three-dimensional Euler aerodynamic method. *Journal of Aircraft* **25**:2, 128-134. [[Citation](#)] [[PDF](#)] [[PDF Plus](#)]
325. CHEN-CHI HSU. A diagonalized TVD scheme for turbulent transonic projectile aerodynamics computation . [[Citation](#)] [[PDF](#)] [[PDF Plus](#)]
326. M. SICLARI, P. DEL GUIDICE. A hybrid finite volume approach to Euler solutions for supersonic flows . [[Citation](#)] [[PDF](#)] [[PDF Plus](#)]
327. PRADEEP RAJ, JAMES BRENNAN. Improvements to an Euler aerodynamic method for transonic flow analysis . [[Citation](#)] [[PDF](#)] [[PDF Plus](#)]
328. M. MACARAEG. Application of CFD to aerothermal heating problems . [[Citation](#)] [[PDF](#)] [[PDF Plus](#)]
329. C. MERKLE. Application of Runge-Kutta schemes to incompressible flows . [[Citation](#)] [[PDF](#)] [[PDF Plus](#)]
330. Pradeep Raj. 1984. A multi-grid method for transonic wing analysis and design. *Journal of Aircraft* **21**:2, 143-150. [[Citation](#)] [[PDF](#)] [[PDF Plus](#)]
331. P. RAJ, J. SIKORA. Free vortex flows - Recent encounters with an Euler code . [[Citation](#)] [[PDF](#)] [[PDF Plus](#)]
332. W. ANDERSON, J. THOMAS, C. RUMSEY. Application of thin-layer Navier-Stokes equations near maximum lift . [[Citation](#)] [[PDF](#)] [[PDF Plus](#)]
333. W. THOMPSON, JR., S. TONG, R. BUSH, W. USAB, JR.. Solution procedures for accurate numerical simulations of flow in turbomachinery cascades . [[Citation](#)] [[PDF](#)] [[PDF Plus](#)]